3. ATMOSPHERIC MEASURMENTS

Markus Rex[1,2], Jürgen Graeser[1], Sandro Dahlke[1,2], Matthew Shupe[3,4], Vagner Castro[5], Steele Griffiths[5], David Chu[5,6], Paul Ortega[5,6], Dean Greenamyer[5], Jody Ellis[5], Janek Uin[5,7], Misha Krassowski[5,8], Matt Boyer[5,7], Todd Houchens[5,9], Jessie Creamean[10], Ola Persson[3,4], Ronny Engelmann[15], David Costa[3,4], Ian Brooks[18], Andreas Preußer[23], Byron Blomquist[3,4], Steve Archer[24], Jacques Hueber[3], Lauriane Quéléver[29], Amelie Kirchgässner[31]

(not on board:) Marion Maturilli[1], Alexander Schulz[1], Heath Powers[5,6], Jim Mather[5,9], Kerri Pratt[11], Gijs de Boer[3,4], Klaus Dethloff[1], Elizabeth Hunke[6], Wieslaw Maslowski[12], Allison McComiskey[7], David Randall[10], Michael Tjernstrom[13], David Turner[4], Johannes Verlinde[14], Hannes Griesche[15], Martin Radenz[15], Julian Hofer[15], Dietrich Althausen[15], Holger Baars[15], Patric Seifert[15], Albert Ansmann[15], Andreas Macke[15], Mario Mech[16], Bernhard Pospichal[16], Kerstin Ebell[16], Susanne Crewell[16], Gaël Dubois[17], Luc Blarel[17], Philippe Goloub[17], Thomas Ayers[4], Christopher Cox[4], Christopher Fairall[4], Michael Gallagher[3,4], Daniel Gottas[4], Jesse Leach[4], Sara Morris[4], Jackson Osborn[3,4], Sergio Pezoa[4], Taneil Uttal[4], Jennifer Hutchings[19], Don Perovich[20], Timothy Stanton[21], Roberta Pirazzini[22], Ryan Neely III[18], Barbara Brooks[18], Günther Heinemann[23], Detlev Helmig[3], Laurens Ganzeveld[25], Dean Howard[3], Ludovich Bariteau[3,4], Kevin Posman[24], Hans-Werner Jacobi[26], Hélène Angot[3], Sjoerd Barten[25], William Sturges[27], Lucy Carpenter[28], Julia Schmale[30], Mikko Sipilä[29], Ivo Beck[30], Tiia Laurila[29], Tuija Jokinen[29], Zoé Brasseur[29], Markus Frey[31], Manuela van Pinxteren[15], Thomas Lachlan-Cope[31], Xin Yang[31], Alice Jones[31], Leon Clarke[32], Paul DeMott[10], Thomas Hill[10]

[1]DE.AWI
[2]DE.UNI-Potsdam
[3]EDU.CU
[4]GOV.NOAA
[5]GOV.ARM
[6]GOV.LANL
[7]GOV.BNL
[8]GOV.ORNL
[9]GOV.SANDIA
[10]EDU.CSU
[11]EDU.UMICH
[12]EDU.NPS
[13]SE.SU
[14]EDU.PSU
[15]DE.TROPOS
[16]DE.UNI-KOELN
[17]FR.UNIV-LILLE
[18]UK.UNI-LEEDS
[19]EDU.ORSU
[20]EDU.DARTMOUTH
[21]EDU.NPS
[22]FI.FMI
[23]DE.UNITRIER
[24]ORG.BIGELOW
[25]NL.WUR
[26]FR.UGA
[27]UK.AC.UEA
[28]UK.AC.YORK
[29]FI.UNI-Helsinki
[30]CH.EPFL
[31]UK.BAS
[32]UK.AC.MMU

Grant-No. AWI_PS122_00

A comprehensive summary of the atmospheric measurements during all 5 cruise legs can be found in Shupe et al., 2022.

References

Shupe, MD, Rex, M, Blomquist, B, Persson, POG, Schmale, J, Uttal, T, Althausen, D, Angot, H, Archer, S, Bariteau, L, Beck, I, Bilberry, J, Bucci, S, Buck, C, Boyer, M, Brasseur, Z, Brooks, IM, Calmer, R, Cassano, J, Castro, V, Chu, D, Costa, D, Cox, CJ, Creamean, J, Crewell, S, Dahlke, S, Damm, E, de Boer, G, Deckelmann, H, Dethloff, K, Dütsch, M, Ebell, K, Ehrlich, A, Ellis, J, Engelmann, R, Fong, AA, Frey, MM, Gallagher, MR, Ganzeveld, L, Gradinger, R, Graeser, J, Greenamyer, V, Griesche,

H, Griffiths, S, Hamilton, J, Heinemann, G, Helmig, D, Herber, A, Heuzé, C, Hofer, J, Houchens, T, Howard, D, Inoue, J, Jacobi, H-W, Jaiser, R, Jokinen, T, Jourdan, O, Jozef, G, King, W, Kirchgaessner, A, Klingebiel, M, Krassovski, M, Krumpen, T, Lampert, A, Landing, W, Laurila, T, Lawrence, D, Lonardi, M, Loose, B, Lüpkes, C, Maahn, M, Macke, A, Maslowski, W, Marsay, C, Maturilli, M, Mech, M, Morris, S, Moser, M, Nicolaus, M, Ortega, P, Osborn, J, Pätzold, F, Perovich, DK, Petäjä, T, Pilz, C, Pirazzini, R, Posman, K, Powers, H, Pratt, KA, Preußer, A, Quéléver, L, Radenz, M, Rabe, B, Rinke, A, Sachs, T, Schulz, A, Siebert, H, Silva, T, Solomon, A, Sommerfeld, A, Spreen, G, Stephens, M, Stohl, A, Svensson, G, Uin, J, Viegas, J, Voigt, C, von der Gathen, P, Wehner, B, Welker, JM, Wendisch, M, Werner, M, Xie, ZQ, Yue, F. 2022. Overview of the MOSAiC expedition: Atmosphere. Elementa: Science of the Anthropocene 10(1). DOI: https://doi.org/10.1525/elementa.2021.00060

3.1 From the surface to the stratosphere: characterization of the atmospheric column

Markus Rex[1,2], Jürgen Graeser[1], Sandro Dahlke[1,2]

(not on board:) Marion Maturilli[1], Alexander Schulz[1]

[1]DE.AWI

[2]DE.UNI-Potsdam

Objectives

a) Characterization of the planetary boundary layer over sea ice

The Planetary Boundary Layer (PBL) is the lowermost atmospheric layer, connecting the surface and the free atmosphere. In the Arctic, and especially during polar night and under high pressure influence, the Arctic PBL is typically a stable and persistent feature. In the case of stable conditions, exchange with the surface is strongly inhibited, and marked temperature inversions of the order of several Kelvin are common features. In case of neutral conditions, both synoptic and radiative forcing can quickly change turbulence characteristics. The turbulent fluxes of momentum, energy and chemical compounds, as well as surface-based temperature inversions in the Arctic PBL are known to be crucial players in Arctic Warming and sea ice retreat, but are generally poorly resolved in state of the art climate models (Boé et al., 2009, Pavelsky et al., 2012, Holtslag et al. 2013,). This is in parts due to insufficient parameterizations of sub-grid scale processes (Pithan et al., 2014) that have been developed on the basis of only a few dedicated campaigns, such as, for instance, AIDJEX (Andreas et al., 1979), LEADEX (Ruffieux et al., 1995), SHEBA (Uttal et al., 2002) or STABLE (Tetzlaff et al., 2015). Other than during these campaigns, the extraordinary opportunity during MOSAiC is to measure characteristics of the Arctic PBL over sea ice during the course of a whole year, including a variety of different surface characteristics. Monitoring the thermal structure of the PBL is enabled by a state of the art *in-situ* sensor for capturing high frequency temperature fluctuations along a fibre cable (Distributed Temperature Sensor, DTS), with 25 cm physical resolution and 10 seconds sampling interval. Using a tethered balloon (TB) as a carrier platform for the DTS, vertical time series of the thermodynamic structure of the PBL will be retrieved, and the potential impact of nearby open leads (open water), ridges (high obstacles) or changing large-scale synoptic forcing will be investigated. This is the first time ever the DTS technology is combined with a TB for such investigations over the central Arctic sea ice. A suite of additional sensors from other partners and institutes will be occasionally deployed with the TB throughout the course of the year, giving additional insights into the dynamical, thermodynamical and chemical characteristics of the PBL onsite the TB launch platform. These include, e.g. an optical particle sonde, an aerosol particle filter package, an ozone profiler, and a turbulence sensor package. The combined measurements assure the close link to other projects and foster the joint analysis of other atmospheric topics.

b) Characterization of the free troposphere and lower stratosphere

An extensive balloon program will operate from board *Polarstern*, reaching from upgraded weather balloons to sophisticated research sondes. The profiles obtained by radiosondes launched four times daily will directly support the on-site weather forecast during the expedition, while they further contribute to numerical weather forecast as observational input for data assimilation. Additional Arctic radiosondes are known to positively impact the performance of forecast systems (Yamazaki et al., 2015; Inoue et al., 2015) even in regions far from the Arctic (Sato et al., 2016; 2018). The atmospheric thermodynamic structure over sea ice was recorded by radiosondes during earlier campaigns like e.g. SHEBA (Uttal et al., 2002) or N-ICE2015 (Kayser et al., 2017) for other regions of the Arctic. Now, the atmospheric structure, moisture content, stability, ABL height, tropopause height and other features in the vertically resolved atmospheric column will be monitored in the Central Arctic for a complete annual cycle. Events of heat and moisture transport into the Arctic by intrusions or atmospheric rivers (Woods and Caballero, 2016; Nash et al., 2018) will be identified, and their impact on the local atmospheric structure analyzed. The combination with projects that focus on the observation of clouds and radiation will allow to focus on the transitions between radiatively clear and cloudy states (Stramler et al., 2011; Graham et al., 2017) and how these transitions impact the vertical stability and coupling within the atmospheric column. The radiosonde profiles retrieved during MOSAiC will be set into context with similar measurements at pan-Arctic land based stations (e.g. Ny-Alesund, Utqiagvik/Barrow, and other IASOA stations) for studies of the advective connection between the inner and outer Arctic, and the role of the Arctic dome in these exchange processes.

Weekly ozone sonde profiles will characterize the ozone distribution in the tropo- and the stratosphere throughout the year. In winter and spring, they will be part of a potential pan-Arctic ozone sonde campaign (Match) with coordinated soundings at all Arctic ozone sonde stations (e.g. von der Gathen et al., 1995; Rex et al., 1997, 2004; Manney et al., 2011). The aim is to determine the ozone loss inside the polar vortex. We expect new Arctic record ozone losses due to record low temperature regimes in single winters within the future 10 to 20 years (e.g. Rex et al., 2006).

Water vapor is a chemically, physically, and radiatively active trace gas, and its distribution in the stratosphere determines significant climatic implications. The water vapor distribution in the Arctic stratosphere bares evidence for dynamical aspects on different scales, including

the large scale descending motion inside the polar vortex as well as filamentary structures at the vortex edge linked to Rossby wave activity (Maturilli et al., 2006). In the presence of very low temperatures, the sedimentation of polar stratospheric cloud (PSC) ice particles can lead to dehydration events (Maturilli and Dörnbrack, 2006; Khaykin et al., 2013). With our monthly balloon-borne cryogenic frostpoint hygrometer (CFH) measurements during MOSAiC we contribute to the assessment of the water vapour distribution in the Arctic stratosphere. The dual soundings with the Compact Optical Backscatter and AerosoL Detector (COBALD) during polar night will allow to identify PSC layers related to dehydration.

Work onboard *Polarstern*

Throughout Leg 1, 286 weather balloons have been started from the Heli deck onboard *Polarstern* in a 6-hourly rhythm. The launch times were chosen after the synoptical hours, i.e. 05UTC, 11UTC, 17UTC and 23UTC. In addition to these standard meteorological radiosondes, joint launches with ozone sensors were conducted roughly on a weekly basis. A list of all ozone soundings during leg 1 is given in Table 3.1.1.

Tab.3.1.1: List of all ozone soundings during leg 1, with device operation (left) and date (right).

PS122/1_2-115	12.10.2019 11UTC
PS122/1_2-142	16.10.2019 11UTC
PS122/1_2-191	23.10.2019 11UTC
PS122/1_5-23	30.10.2019 11UTC
PS122/1_6-27	06.11.2019 11UTC
PS122/1_8-14	19.11.2019 11UTC
PS122/1_9-21	26.11.2019 11UTC
PS122/1_10-31	04.12.2019 11UTC
PS122/1_11-33	11.12.2019 17UTC

The sounding PS122/1_8-14 furthermore incorporates a launch of the CFH and COBALD.

Work on the ice

For the operation of the tethered balloon (TB), a dedicated launch site, called Balloon Town (BT), has been installed in the Central Observatory, close to Ocean City, at approximately 400 m distance to *Polarstern.* The location of BT was chosen by taking into account a long enough "emergency take down" pathway by skidoo for the TB, and a sufficient distance to the Heli Deck on *Polarstern.*

Fig.3.1.1: Balloon Town

BT consists of 2 tents and 2 launch platforms (see Figure 3.1.1). The first tent is a large, unheated one, that provides shelter for the 9 m^3 TB and its operational and scientific equipment, whenever it is not in operation. The 2 launch platforms have been mounted

approximately 4 m east and west of this tent, such that the most suitable one for each launch could be chosen according to the wind direction during the TB operation.

The second tent is a smaller, heated tent that allows storage and operation of frost-sensitive items, such as laptops, and provides more comfortable conditions for working over longer times.

Upon finishing the construction of the site, balloon launches followed according to the wind conditions. Launches were only conducted when the surface winds were less than 6 m/s, and the wind speed in the vicinity of the low-level jet in some hundred m height did not exceed 10m/s.

The TB has a payload of 4-5 kg and was operated via a winch up to 1500 m altitude. During leg 1, an overall number of 7 TB launches was conducted, and 3 different sensors were deployed during those flights, including a tethersonde for standard meteorology, the turbulence sensor package, and the DTS. A list of all TB launches and deployed sensors is given in Table 3.1.2.

Tab.3.1.2: List of all TB operations during leg 1.

Device operation	**Sensor**	**Start time UTC**	**End time UTC**	**Max. altitude**
PS122/1_8-84	Tethersonde	21.11.2019 10:15	21.11.2019 10:55	1040 m
	Turbulence	21.11.2019 10:15	21.11.2019 10:55	1040 m
PS122/1_8-99	Tethersonde	22.11.2019 08:53	22.11.2019 09:40	925 m
	Turbulence	22.11.2019 08:53	22.11.2019 09:40	925 m
PS122/1_10-90	Tethersonde	06.12.2019 12:17	06.12.2019 12:37	1322 m
	Turbulence	06.12.2019 12:17	06.12.2019 12:37	1322 m
PS122/1_10-91	Tethersonde	06.12.2019 18:15	06.12.2019 19:18	1553 m
	Turbulence	06.12.2019 18:15	06.12.2019 19:18	1553 m
PS122/1_10-92	Tethersonde	07.12.2019 06:05	07.12.2019 06:24	568 m
	Turbulence	07.12.2019 06:05	07.12.2019 06:24	568 m
PS122/1_11-34	Tethersonde	11.12.2019 12:58	11.12.2019 13:50	
	Turbulence	11.12.2019 12:58	11.12.2019 13:50	
PS122/1_11-47	Tethersonde	12.12.2019 07:41	12.12.2019 13:46	362 m
	Turbulence	12.12.2019 07:41	12.12.2019 09:55	362 m
	DTS	12.12.2019 08:21	12.12.2019 12:48	362 m

Preliminary results

The comprehensive record of radiosondes gives insight into the temporal evolution of meteorological key parameters over the atmospheric column from the near surface layers up to the stratosphere, and provides a linkage to larger-scale processes in the atmosphere. Measured parameters include temperature, relative humidity, wind speed and direction. Figure 3.1.2 shows a sequence of temperatures and wind speeds as deduced from the soundings of leg 1. On average, soundings reached altitudes of 25-30 km. Temperature fluctuations are evident in both troposphere and stratosphere. Using the detection criterion of a reversing vertical temperature gradient, the tropopause is in many cases well established around 10 km height.

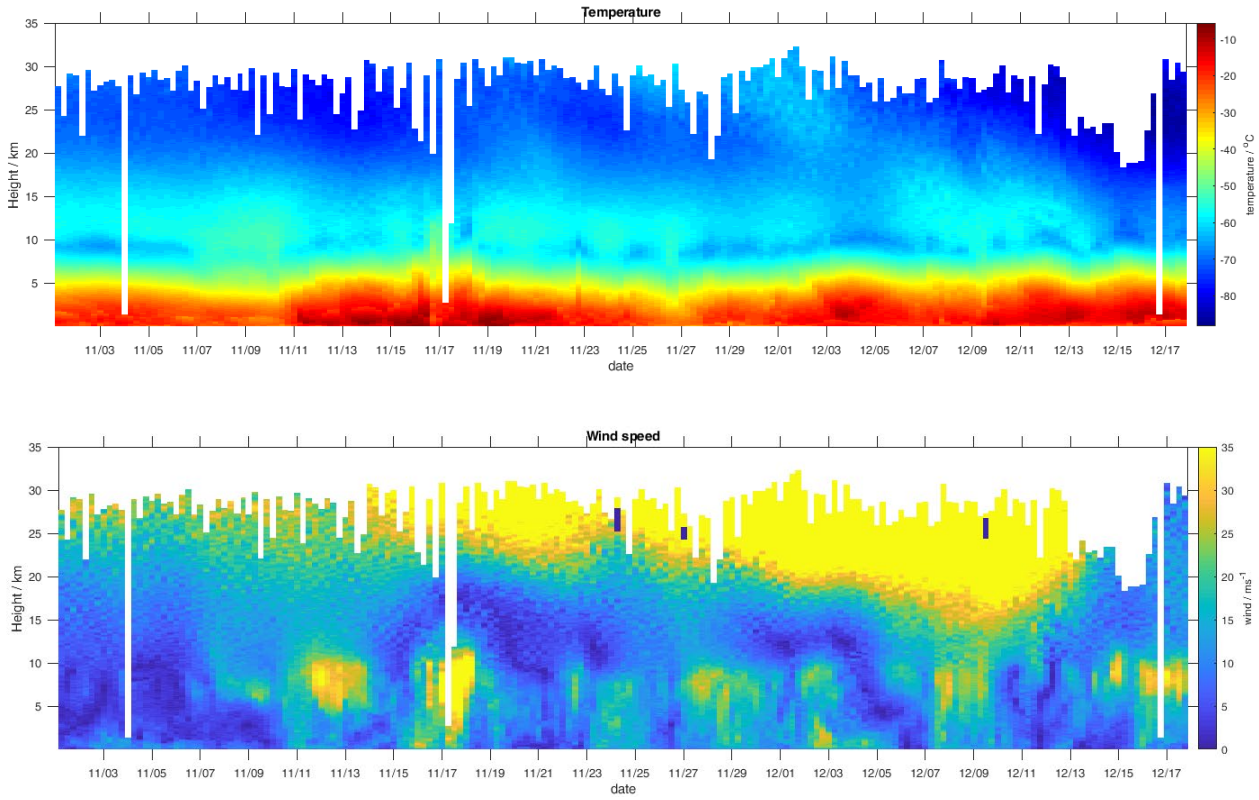

Fig.3.1.2: time-height sections of temperature (top) and absolute wind speed (bottom) from leg 1 soundings.

Wind profiles illustrate the buildup of the stratospheric polar vortex throughout the course of leg 1, given the steadily increasing winds in the upper few kilometers of the sounding profiles. In the troposphere and partially extending vertically towards the surface, evidence is provided for the passage of cyclones and the associated strong winds events, that occurred on 16-18 November and 2-4 December and that had lead to noteworthy deformations of the Central Observatory.

Towards the end of leg 1, a marked drop in upper stratospheric temperatures down to -87°C is detected, that goes along with a pronounced decrease in wind speeds. This may indicate that the corresponding soundings profiled the inner vortex.

Figure 3.1.3 shows time series of ozone partial pressure as deduced from the leg 1 ozone soundings. A generally increasing tendency is apparent, resembling the buildup of the Arctic ozone layer between 15-20 km height, which is consistent with the cooling trend in the stratosphere and with the strengthening of the polar vortex throughout leg 1. The sounding on 11 December, however, reveals reduced ozone values, particularly between 15-19 km altitude. Comparison with the wind profiles from Figure 3.1.2 indicates that the layer of reduced ozone concentrations was subject to strong winds and strong vertical wind shear. This may point towards the close proximity to the edge of the polar vortex, and the hence less ozone-rich air.

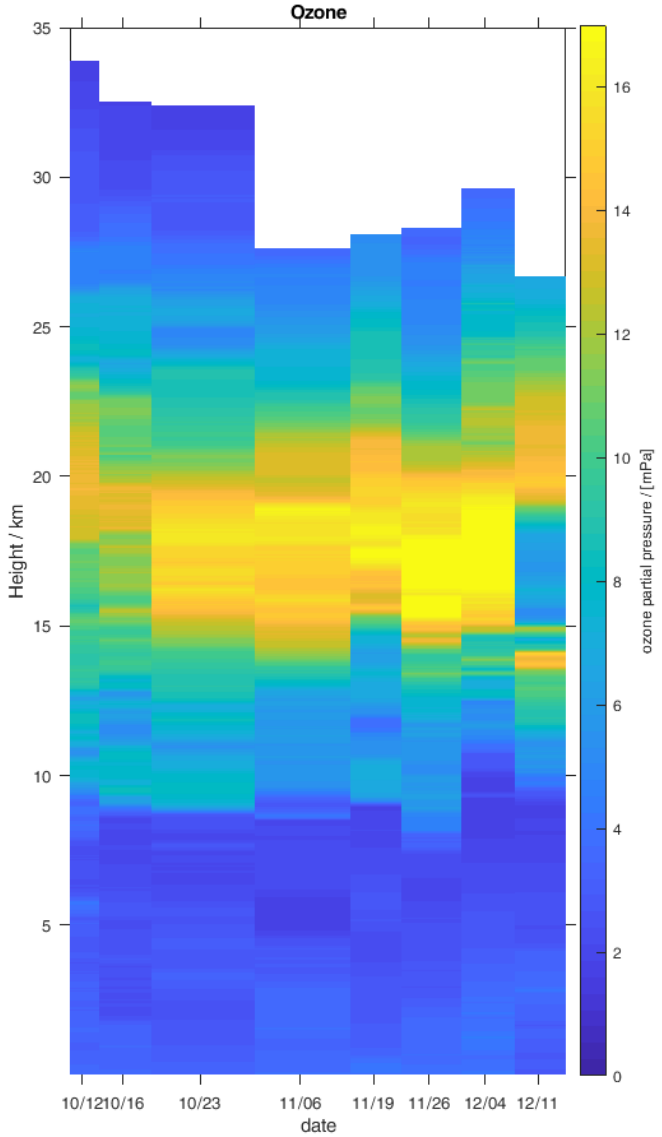

Fig.3.1.3: Time-height section of ozone soundings during leg 1.

Data management

All data are handled, documented, archived and published following the MOSAiC data policy (see APPENDIX). All radiosonde data have been transmitted to the GTS in near real-time to assure their availability for numerical weather forecast. All sounding data (radiosonde, ozone sonde, CFH, COBALD) and according auxiliary measurements are stored in the MCS. Upon the end of leg 1, the preliminary sounding data will be processed at the GRUAN Lead Centre in Lindenberg, Germany. The final sounding data will be made available via the PANGAEA data repository according to the MOSAiC Data Policy.

The DTS light backscatter profiles (incl. preliminary temperature profiles were also stored in the MCS after each measurement period. The final data processing of the DTS temperature profiles will be conducted at the Alfred Wegener Institute in Potsdam, Germany (contact: Alexander Schulz, alexander.schulz@awi.de). Final data products will be stored at the PANGAEA data repository (World Data Center PANGAEA Data Publisher for Earth & Environmental Science (www.pangaea.de)).

References

Andreas EL, Paulson CA, William RM, Lindsay RW, Businger JA. 1979. The turbulent heat flux from arctic leads. Boundary-Layer Meteorol. 17, 57–91

Boé J, Hall A, Qu X (2009) Current GCMs' Unrealistic Negative Feedback in the Arctic. Journal of Climate, 22, 4682-4695

Graham R, Rinke A, Cohen L, Hudson SR, Walden VP, Granskog MA, Dorn W, Kayser M, and Maturilli M (2017) A comparison of the two Arctic atmospheric winter states observed during N-ICE2015 and SHEBA, J. Geophys. Res. Atmos., 122, 5716–5737

Holtslag AAM, Svensson G, Baas P, Basu S, Beare B, Beljaars ACM, Bosveld FC, Cuxart J, Lindvall J, Steeneveld GJ, Tjernström M, Van De Wiel BJH (2013) Stable Atmospheric Boundary Layers and Diurnal Cycles: Challenges for Weather and Climate Models. BAMS, 1691-1706

Inoue J, Yamazaki A, Ono J, Dethloff K, Maturilli M, Neuber R, Edwards P, and Yamaguchi H (2015) Additional Arctic observations improve weather and sea-ice forecasts for the Northern Sea Route, Science Reports, 5, 16868

Kayser M, Maturilli M, Graham RM, Hudson SR, Rinke A, Cohen L, Kim J-H, Park S-J, Moon W, Granskog, M (2017). Vertical thermodynamic structure of the troposphere during the Norwegian young sea ICE expedition (N-ICE2015). Journal of Geophysical Research: Atmospheres 122.20, 10855–10872.

Khaykin SM, Engel I, Vömel H, Formanyuk IM, Kivi R, Korshunov LI, Krämer M, Lykov AD, Meier S, Naebert T, Pitts MC, Santee ML, Spelten N, Wienhold FG, Yushkov VA, and Peter T (2013), Arctic stratospheric dehydration – Part 1: Unprecedented observation of vertical redistribution of water, Atmos. Chem. Phys., 13, 11503-11517

Maturilli M, and Dörnbrack A (2006) Polar stratospheric ice cloud above Spitsbergen, J. Geophys. Res., 111, D18210

Maturilli M, Fierli F, Yushkov V, Lukyanov A, Khaykin S, and Hauchecorne A (2006) Stratospheric Water vapour in the vicinity of the Arctic polar vortex. Annales Geophysicae, 24, 1511-1521

Manney GL, Santee ML, Rex M, Livesey NJ, Pitts MC, Veefkind P, Nash ER, Wohltmann I, Lehmann R, Froidevaux L, Poole LR, Schoeberl MR, Haffner DP, Davies J, Dorokhov V, Gernandt H, Johnson B, Kivi R, Kyrö E, Larsen N, Levelt PF, Makshtas A, McElroy CT, Nakajima H, Parrondo MC, Tarasick DW, von der Gathen P, Walker KA, and Zinoviev NS (2011) Unprecedented Arctic ozone loss in 2011, Nature, 478 (7370), pp. 469-475

Nash D, Waliser D, Guan B, Ye H, and Ralph F (2018) The role of atmospheric rivers in extratropical and polar hydroclimate, J. Geophys. Res. Atmos., 123, 6804–6821

Pavelsky TM, Boé J, Hall A, Fetzer, EJ (2011) Atmospheric inversion strength over polar oceans in winter regulated by sea ice. Climate Dynamics, 36, 945-955

Pithan F, Medeiros B, Mauritsen T (2014) Mixed-phase clouds cause climate model biases in Arctic wintertime temperature inversions. Climate Dynamics, 43, 289-303

Rex M, Harris NRP, von der Gathen P, Lehmann R, Braathen GO, Reimer E, Beck A, Chipperfield MR, Alfier R, Allaart M, O'Connor F, Dier H, Dorokhov V, Fast H, Gil M, Kyrö E, Litynska Z, Mikkelsen IS, Molyneux MG, Nakane H, Notholt J, Rummukainen M, Viatte P, and Wenger J (1997) Prolonged stratospheric ozone loss in the 1995/96 Arctic winter, Nature, 389 , pp. 835-838

Rex M, Salawitch RJ, von der Gathen P, Harris NRP, Chipperfield M, and Naujokat B (2004) Arctic ozone loss and climate change, Geophys. Res. Lett., 31, L04116

Rex, M, Salawitch RJ, Deckelmann H, von der Gathen P, Harris NRP, Chipperfield MP, Naujokat B, Reimer E, Allaart M, Andersen SB, Bevilacqua R, Braathen GO, Claude H, Davies J, De Backer H, Dier H, Dorokov V, Fast H, Gerding M, Hoppel K, Johnson B, Kyrö E, Litynska Z, Moore D, Nagai T, Parrondo MC, Risley D, Skrivankova P, Stübi R, Trepte C, Viatte P, and Zerefos C (2006) Arctic winter 2005: Implications for stratospheric ozone loss and climate change , Geophysical Research Letters, 33, L23808

Ruffieux D, Persson, POG, Fairall CW, Wolfe DE. 1995. Ice pack and lead surface energy budgets during LEADEX 1992. J. Geophys. Res. 100, 4593–4612

Sato K, Inoue J, Yamazaki A, Kim J-H, Maturilli M, Dethloff K, Hudson SR, and Granskog MA (2016) Improved forecasts of winter weather extremes over midlatitudes with extra Arctic observations, J. Geophys. Res. Oceans, 121

Sato K, Inoue J, Yamazaki A, Kim J-H, Makshtas A, Kustov V, Maturilli M, and Dethloff K (2018) Impact on predictability of tropical and mid-latitude cyclones by extra Arctic observations, Science Reports, 8, 12104

Stramler K, Genio ADD, and Rossow WB (2011) Synoptically driven Arctic winter states, Journal of Climate, 24(6), 1747–1762

Tetzlaff A, Lüpkes C, and Hartmann J (2015) Aircraft-based observations of atmospheric boundary-layer modification over Arctic leads, Quarterly Journal of the Royal Meteorological Society

Uttal, T, and Coauthors (2002): Surface heat budget of the Arctic Ocean. Bull. Amer. Meteor. Soc., 83, 255–275

von der Gathen P, Rex M, Harris NRP, Lucic D, Knudsen BM, Braathen GO, Backer HD, Fabian R, Fast H, Gil M, Kyrö E, Mikkelsen IS, Rummukainen M, Stähelin J, and Varotsos C (1995) Observational evidence for chemical ozone depletion over the Arctic in winter 1991-92, Nature, 375, pp. 131-134

Woods C, and Caballero R (2016) The role of moist intrusions in winter Arctic warming and sea ice decline, Journal of Climate, 29(12), 4473–4485

Yamazaki A, Inoue J, Dethloff K, Maturilli M, and König-Langlo G (2015) Impact of radiosonde observations on forecasting summertime Arctic cyclone formation, J. Geophys. Res. Atmos., 120

3.2 DOE Atmospheric Radiation Measurement program's mobile facility

Matthew Shupe[1,2], Vagner Castro[3], Juarez Viegas[3], Steele Griffiths[3], David Chu[3,4], Paul Ortega[3,4], Dean Greenamyer[3], Jody Ellis[3], Janek Uin[3,5], Misha Krassowski[3,6], Matt Boyer[3,5], Todd Houchens[3,7], Jessie Creamean[8], Ola Persson[1,2]

(not on board:) Heath Powers[3,4], Jim Mather[3,7], Kerri Pratt[9], Gijs de Boer[1,2], Klaus Dethloff[10], Elizabeth Hunke[4], Wieslaw Maslowski[11], Allison McComiskey[5], David Randall[8], Michael Tjernstrom[12], David Turner[2], Johannes Verlinde[13]

[1]EDU.CU
[2]GOV.NOAA
[3]GOV.ARM
[4]GOV.LANL
[5]GOV.BNL
[6]GOV.ORNL
[7]GOV.SANDIA
[8]EDU.CSU
[9]EDU.UMICH
[10]DE.AWI
[11]EDU.NPS
[12]SE.SU
[13]EDU.PSU

Objectives

To understand the changing Arctic sea ice at a fundamental level requires a detailed accounting of energy flow through the sea ice system. While it is clear that atmospheric energy fluxes are critically important for the sea ice energy budget, many processes controlling these fluxes, and their interactions, are poorly understood and represented in numerical models. This project aims to observe specific processes that control the flow of energy through the Arctic atmospheric system and thereby to address pressing science questions under four broad topics.

(a) Surface Energy Budget: What is the annual evolution of the surface energy budget over young sea ice? What are the key process interactions determining the surface energy budget and specifically variability in surface radiation?

(b) Clouds and Precipitation: What factors determine Arctic cloud phase partitioning? What role do clouds and precipitation play in determining low-level atmospheric structure? How does surface inhomogeneity influence the spatial structure of cloud-precipitation systems?

(c) Aerosols: How do aerosol physical, chemical, and optical properties over sea ice vary seasonally? What sources and transport patterns are responsible for variability in Arctic aerosol? What are the radiative and cloud-nucleating properties of Arctic aerosol?

(d) Boundary Layer Structure: What are the properties and effects of stably stratified turbulence in the Arctic boundary layer? What are the effects of a thinned ice cover on boundary layer stability and heat fluxes? How do surface- and cloud-driven dynamics impact the boundary layer structure?

Work at sea

To provide the diverse and detailed atmospheric measurements needed to address the primary scientific objectives of the project, the US Department of Energy's Atmospheric Radiation Measurement (ARM) Program (www.arm.gov) has deployed its second ARM Mobile Facility (AMF-2) onboard and nearby *Polarstern* during MOSAiC. This extensive suite of instruments is operated in a collection of six laboratory sea-containers installed on the bow of *Polarstern*, one laboratory container installed on the *Polarstern* P-deck, as well as various instruments installed at Met City out on the sea ice of the Central Observatory. ARM has also provided funding support for one half of the meteorological radiosonde program led by AWI during MOSAiC, as well as personnel support for launching some of these soundings. The AMF-2 facility can be described via five instrument collections, which are captured in Table 3.2.1.

Tab.3.2.1. All instruments installed and operated by the DOE ARM program, including the measurement objectives, installation location, and start date for observations.

Instrument	Measurement Objectives	Installation Location	Start of Observations
Meteorology and Winds			
Radiosonde Program (support for ½ of equipment)	Profiles of temperature and humidity	Helideck	20 Sept
Present Weather Detector (PWD)	Visibility	(1) P-deck port side; (2) Met City	17 Oct
Beam-steerable radar wind profiler (BSRWP)	Wind profiles	KAZR lab (C3)	5 Oct
Doppler lidar (DL)	Wind profiles, turbulence	Top OPS lab (C4)	7 Oct
Cloud Properties and Processes			
2-channel microwave radiometer (MWR2C)	Liquid water path and precipitable water vapor	Lower P-deck port side	16 Oct
3-channel microwave radiometer (MWR3C)	Liquid water path and precipitable water vapor	Lower P-deck port side	8 Oct
Ka-Band ARM Zenith Radar (KAZR)	Cloud occurrence and properties	KAZR lab (C3)	5 Oct
Marine W-Band ARM Cloud Radar (MWACR)	Cloud occurrence and properties	Top of OPS lab (C4)	16 Oct
High Spectral Resolution Lidar (HSRL)	Cloud & aerosol properties	OPS lab (C4)	10 Oct
Micropulse Lidar (MPL)	Cloud & aerosol properties	OPS lab (C4)	5 Oct
Ceilometer (CEIL)	Cloud base height	Lower P-deck port side	8 Oct
Total Sky Imager (TSI)	Hemispheric sky views	P-deck	Not installed

Precipitation			
Ka-Band Scanning ARM Cloud Radar (Ka-SACR)	Cloud and precipitation spatial distribution	P-deck, starboard side	5 Oct
Parsivel2 Laser Disdrometer (LDIS)	Fall velocity and precipitation rate of precipitation	(1)P-deck port side; (2)Met City double Altar shield	(1) 30 Oct, (2) 14 Nov
Pluvio2 Weighing Bucket Rain Gauge (WBRG)	Precipitation mass	Met City in double Altar shield	30 Oct
Siphon Rain Gauge (SRG)	Precipitation mass	P-deck port side	30 Oct
Radiation			
Marine Atmospheric Emitted Radiance Interferometer (MAERI)	Spectral infrared radiation, both downwelling and upwelling	Lower P-deck port side, view to port side ice	9 Oct
Cimel Sunphotometer (CSPHOT)	Atmospheric transmission & scattering during daylight	P-deck	Not yet installed
Fast Rotating Shadowband Radiometer (FRSR)	Direct and diffuse components of downward solar flux	P-deck	14 Oct
Ground Radiometer System (GNDRAD) – PIR, PSP	Upwelling shortwave and longwave radiation	Met City “swingset”	14 Oct
Ground Infrared Thermometer (IRT)	Ground temperature with wide field-of-view	Met City “swingset”	30 Oct
Multifilter Radiometer 3-meter (MRF3M)	Reflected radiative flux in narrow bands	Met City “swingset”	14 Oct
Ice Radiometer System (ICERAD) – PIR, PSP, SPN1	Downwelling shortwave and longwave radiation, with shortwave direct and diffuse	Met City	14 Oct
Shipboard Radiometer System (SHIPRAD) – PIR, PSP, SPN1	Downwelling shortwave and longwave radiation, with shortwave direct and diffuse	(1) P-deck port side; (2) P-deck starboard side	(1) 7 Oct; (2) 7 Oct
Sky Infrared Thermometer (IRT)	Sky temperature with narrow field-of-view	Met City “swingset”	14 Oct
Aerosols and Gases			
Automated Weather Station (AOSMET)	Pressure, temperature, relative humidity, winds	AOS inlet on AOS lab (C5)	9 Oct
Trace Gas Monitors	Concentrations: carbon monoxide, nitrous oxide, water vapor	AOS lab (C5)	9 Oct
Ozone Monitor	Concentration of ozone	AOS lab (C5)	9 Oct

Aerosol Chemical Speciation Monitor (ACSM)	Bulk chemical composition	AOS lab (C5)	8 Nov
Condensation Particle Counter (CPC)	Total particle concentration for sizes >10nm	AOS lab (C5)	8 Oct
Ultrafine Condensation Particle Counter (UCPC)	Total particle concentration for sizes >3nm	AOS lab (C5)	8 Oct
Cloud Condensation Nuclei Counter (CCN)	Concentration of cloud condensation nuclei	AOS lab (C5)	8 Nov
Scanning Mobility Particle Sizer (SMPS)	Aerosol size distribution	AOS lab (C5)	9 Oct
Ultra-High Sensitivity Aerosol Spectrometer (UHSAS)	Aerosol size distribution	AOS lab (C5)	7 Oct
Humidified Tandem Differential Mobility Analyzer (HTDMA)	Aerosol size distribution exposed to different moisture levels	AOS lab (C5)	28 Sept
Single Particle Soot Photometer (SP2)	Soot mass of aerosol particles	AOS lab (C5)	15 Oct
Particle Soot Absorption Photometer (PSAP)	Bulk aerosol absorption	AOS lab (C5)	8 Oct
Nephelometer (NEPH)	Total aerosol scattering at 450, 550, and 700 nm wavelengths	AOS lab (C5)	8 Oct

In addition to the core AMF-2 instruments, ARM has agreed via a proposal process to host and operate instrumentation for two collaborating scientists, Drs. Jessie Creamean and Kerri Pratt. These guest instruments complement the core ARM measurements by the addition of ice nucleus filters, drum samplers, and impactors, all sampling off of the Aerosol Observing System's inlet (see section 3.9 for more details).

The ARM facility was supported on MOSAiC Leg 1 by 3 on-site technicians (Castro, Viegas, Griffiths), along with 8 additional deployment personnel for Leg 1a. With a diverse collection of talents and skills, these personnel were essential for setting up such a large suite of instrumentation, and also played a key role in the overall set up of the ice camp and ship scientific instrumentation. The DOE Atmospheric System Research (ASR) Program supported the participation of principle investigator Shupe during Leg 1 to support ARM and other coordination/installation activities. Participation of Creamean and Pratt is also supported by the ASR Program (although Creamean's participation on Leg 1 was supported by a distinct project).

Installation for Leg 1 started several weeks prior to the departure of *Polarstern* from Tromso. ARM personnel implemented a nearly full installation of the AMF-2 equipment on the dockside in Tromso to address any final implementation details and to ensure proper operation of equipment. The equipment was then uninstalled to the point that it could be transported to, and loaded on, *Polarstern*, where some final installations were accomplished in Tromso port. All equipment was then secured for safe transport across the Arctic Ocean and into the ice pack. Equipment was not operated during the journey into the ice pack, although once *Polarstern* was traveling within the ice pack (i.e., minimal pitch and roll), full installations on many systems were completed. Instruments were generally not started until *Polarstern* was parked at its final resting location, primarily because the ARM data system as not started until

that point. Most onboard installations were thus turned on and started collecting measurements during the week of 7 October 2019. ARM radiation and precipitation equipment installed on the sea ice at Met City became operational during the week of 14 October 2019.

Operations during Leg 1 were generally robust, with the following issues.

- The X-band Scanning ARM Cloud Radar (X-SACR) system never operated robustly in spite of many attempts to replace, fix, or modify different components; thus, the only scanning radar system available is the Ka-band component of the SACR.
- The Ka-SACR has been operational for all of Leg 1. Initially it performed a set of scan patterns including full azimuthal scans (PPI) from -90 to +180 degrees (with 0 degrees being defined as forward on *Polarstern*) at 18 different elevation angles ranging from near 0 to 60 degrees; the -90 to -180 degree sector was not included due to ship infrastructure including the Crow's Nest and smokestack. In addition, the radar was scanned from elevation angles of 0 to 90 degrees (RHI) at a set of specific azimuth angles, including 0, 30, 60, 90, 210 degrees relative to forward. The 210 degree RHI was directly between the Crow's Nest and smokestack, but was eventually removed from the strategy due to concerns about interference with ship's equipment. Additionally, near the end of Leg 1, the scan strategy was modified such that the PPI scans at elevation angles less than 10 degrees would be blanked between the azimuth angles of -10 to +20 degrees to limit any direct illumination of the ship's spotlight that was almost directly forward of the radar.
- During the week of 16 November, ARM's equipment at Met City had temporary outages as all equipment at Met City was operated on short-term generators during this period when the power line from the ship was disconnected.
- The AOS system samples air through an inlet and has a special design to minimize sampling of ship's exhaust; this includes monitoring parameters like carbon monoxide to trigger a back flow through the stack during periods of pollution. Thus, for certain periods, typically determined by wind direction, aerosol sampling was not possible.
- Other short-term issues with ARM instrumentation include temporary interruptions to operations of the MWR2C, MAERI, BSRWP to address or change components or systems. Otherwise, all systems operated rather robustly for the duration of Leg 1.

Preliminary (expected) results

Primary results from the AMF-2 deployment at MOSAiC will be an extensive collection of high-quality data sets from the AMF-2 instrumentation that are as continuous as possible for the full year. These data sets will be quality assured by a large team of instrument mentors and facility managers that will not participate in the field at MOSAiC. Based on these data sets, a suite of value-added products will also be derived to provide information on geophysical parameters related to the atmospheric state, clouds, aerosols, vertical atmospheric structure, and others. These data sets are intended to support a great deal of process-based research in support of advancing knowledge, assessing models, and developing improved models for representing climate processes.

Selected example results from MOSAiC Leg 1 include the following. A comprehensive set of radiation measurements were obtained at multiple locations on the ship and sea ice. An example two weeks of broadband longwave radiation measurements are shown in Figure 3.2.1, where the downwelling radiation is shown in orange and the upwelling radiation is shown in blue. Upwelling longwave radiation is proportional to the surface temperature and varies accordingly, with generally warmer temperatures when clouds are present and colder temperatures when the skies are clear. The downwelling radiation varies between two different

states; generally lower fluxes from clear skies and relatively higher fluxes from cloudy skies. The difference between these curves is the net surface longwave radiation, which, in winter, is the primary radiative influence on the surface energy budget.

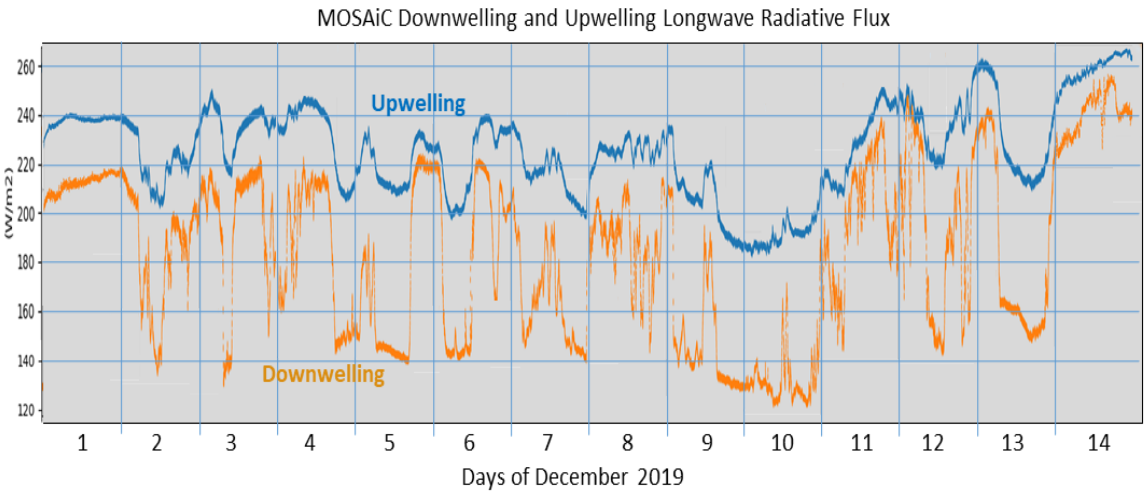

Fig.3.2.1: Timeseries of downwelling (orange) and upwelling (blue) broadband longwave radiative flux as measured by surface based radiometers installed at Met City during MOSAiC Leg 1.

The Ka-band ARM Zenith Radar (KAZR) has observed a consistent record of tropospheric clouds that have advected over the MOSAiC observatory during Leg 1. A timeseries of reflectivity observations is shown in Figure 3.2.2, where the dates for each panel have been provided, and the vertical extent of each panel is from the surface up to approximately 8 km. Reflectivities greater than 0 dBZ are given in yellow and orange colors and represent periods when appreciable snowfall occurs. This timeseries of clouds shows the frequent occurrence of mixed-phase clouds, or clouds that consist of supercooled liquid water in combination with ice crystals.

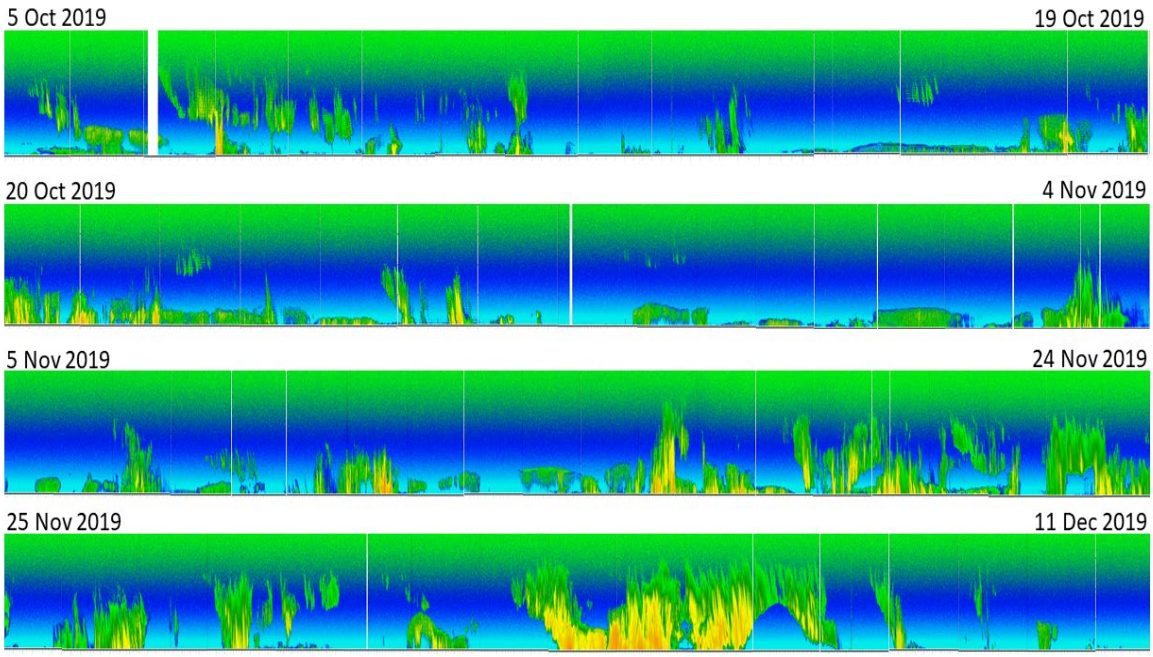

Fig.3.2.2: Timeseries of KAZR cloud reflectivities during Leg 1 of MOSAiC. The vertical extent of the panels is 0-8 km.

Arctic aerosol properties are not well understood in terms of their number concentrations, sources, composition, or cloud activity. One week of observations of particle number concentrations from four distinct measurement systems, each with a unique observational approach, are summarized in Figure 3.2.3. While, subtle differences among the instruments for total number concentration are expected based on the distinct observational approaches, the instrument generally agree on the total aerosol concentrations. This example timeseries shows some interesting aspects of the Leg1 aerosol. First, the large peaks on 2 and 4 November are likely due to ship exhaust, causing very large total number concentrations that are not representative of the Arctic environment. On the other hand, the rest of this timeseries shows the type of variability that is more representative, with values often around 100 cm^{-3}. On 2 November total number concentrations dipped below 1 cm^{-3}, which is remarkably clean; the central Arctic is one of the only locations on Earth that can experience such clean air.

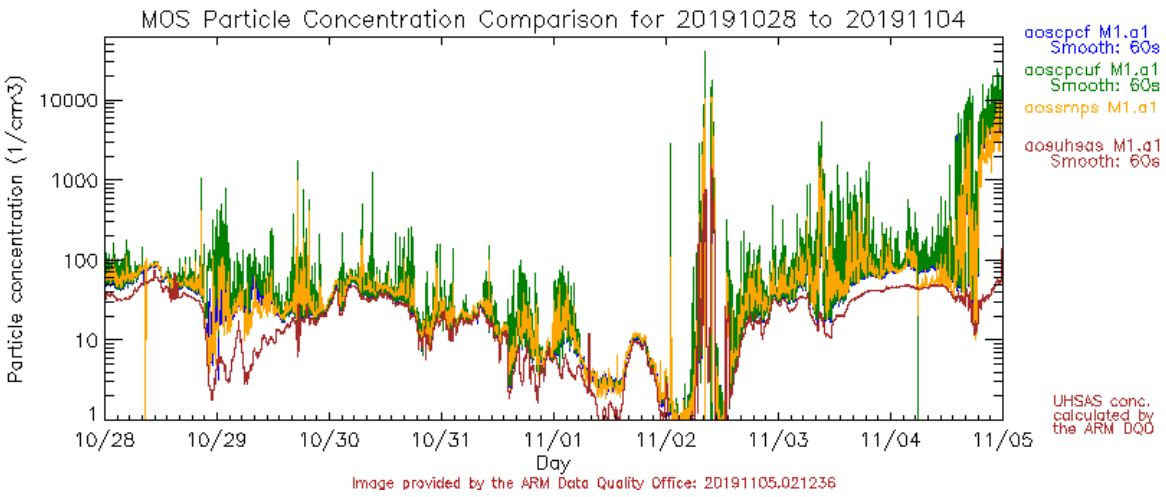

Fig.3.2.3: Timeseries of total aerosol number concentration derived from the CPC, UCPC, SMPS, and UHSAS.

Data management

All data produced by the ARM Program during MOSAiC Leg 1 has been automatically ingested and stored on ARM's onboard "site data system," which performs many operational tasks involved with data management, initial data ingesting and formatting, data quality checks, and the production of quicklook plots of the data. Quicklooks are available via a web page to other scientists onboard *Polarstern* (https://192.168.3.33:8443) and to the general public (https://dq-amfc2.amf.arm.gov). With nearly 20 TB of data produced during Leg 1, it has been agreed that this data will not initially be uploaded to the MOSAiC Central Server, however, MOSAiC scientists can get access to the raw data through a free account on ARM's site data system (192.168.3.33:22) by obtaining credentials from the ARM data manager (see ARM technicians onsite). After MOSAiC Leg 1, and all subsequent legs, the full set of collected data are physically transported to the ARM data management facility and promptly ingested into a full set of processed data files that will then be publicly available via the ARM Data Archive (www.archive.arm.gov). Raw data will be available within a couple of weeks of its arrival at the data management facility. Based on this raw data, a suite of value-added products will also be developed in the following months, with these products also being served at the ARM Archive. Appropriate meta-data sharing and cross-linking will occur via the MOSAiC Central Storage and with PANGAEA (World Data Center PANGAEA Data Publisher for Earth & Environmental Science (www.pangaea.de)) according to the protocol agreed upon between these two archives.

References

No references

3.3 TROPOS – OCEANET: Remote sensing of the annual cycle of aerosol, cloud, and corresponding radiation closure studies in the central arctic

Ronny Engelmann[1],

(not on board:) Hannes Griesche[1], Martin Radenz[1], Julian Hofer[1], Dietrich Althausen[1], Holger Baars[1], Patric Seifert[1], Albert Ansmann[1], Andreas Macke[1], Mario Mech[2], Bernhard Pospichal[2], Kerstin Ebell[2], Susanne Crewell[2], Gaël Dubois[3], Luc Blarel[3], Philippe Goloub[3]

[1]DE.TROPOS

[2]DE.UNI-KOELN

[3]FR.UNIV-LILLE

Objectives

Measurements of the atmospheric state in the Arctic are extremely rare and of great interest for climate research in this unique and changing environment. The mobile facility OCEANET is an ongoing observational initiative of TROPOS for aerosol and cloud profiling as well as radiation budget measurements in maritime environments onboard research vessels since 2007 (Kanitz et al., 2013, Bohlmann et al., 2018). During MOSAiC PS122/1 the majority of these state-of-the-art en-route measurements were implemented on *Polarstern* in order to establish a full Arctic annual aerosol, cloud, and radiation data record. One of the key focusses for TROPOS lies on heterogeneous ice formation processes in different areas of the world (e.g., Kanitz et al, 2011) and their radiative impact.

The following research question are addressed within this project:

- How do aerosol- and cloud properties influence the annual cycle of short-wave and long-wave radiation under different meteorological conditions in the Arctic?

- How often does ice formation in warm (T > –10 °C) stratus clouds occur and what are possible freezing mechanisms under clean Arctic conditions?
- Can we observe different ice-formation rates in the presence of local and long-range transported ice nucleating particles?
- Will Arctic clouds increase or suppress the currently observed Arctic warming?

An additional focus is on ESA's Aeolus wind mission. OCEANET data will also support the CAL/VAL activities of this lidar satellite within the EVAA project. Since it is a polar-orbiting satellite, a large number of overpasses in the close vicinity of *Polarstern* occurred during PS122/1.

Work at sea

The OCEANET container of TROPOS was installed on the bow of *Polarstern* at the container location C8, already during the harbor time in Tromsö. Power, heating, and LAN were connected. However, the installation of instruments on the container's roof was not performed because of the danger of sea-water and waves damaging the instruments at the bow. The setup of all instruments was started at arrival in the sea ice but no en-route measurements were possible at that time because of *Polarstern's* location in the EEZ of Russia. After that, first measurements started on 28 September 2019 already on the way to the ice floe.

Since then continuous measurements with the

- the multi-wavelength Raman depolarization lidar Polly-XT (Engelmann et al., 2016),
- the microwave radiometers HATPRO and LHUMPRO,
- the CIMEL sun/sky/lunar photometer (Yin et al., 2019),
- two disdrometers, Parsivel² and 2DVD,
- a total-sky imager,
- a pyranometer and a pyrgeometer,
- and a basic DWD weather station (T,p,r.h.) were performed.

During the cruise all instruments had to be monitored for operation and several maintenance and calibration tasks were performed. For example, the laser of Polly-XT, needed a flash lamp replacement and an optics cleaning and replacement procedure which resulted in a technical downtime of about 8 hours for the lidar in total. Additional periods with no lidar operation were mainly caused by crane operations above the OCEANET container. The OCEANET platform was installed opposite to the ARM radar container at the bow of *Polarstern* after final installation of all instruments at the top of the container as seen in Figure 3.3.4.

Fig.3.3.1: Location of the OCEANET container (right) and the ARM Radar Container (opposite left) at the bow of Polarstern.

At the beginning of the measurements and during the changeover to Leg 2 the microwave radiometers were calibrated with liquid nitrogen. It was known, that the LN2 generated on board would contain a certain percentage of oxygen and thus the boiling temperature would be different depending on the purity. Hence, the temperature of the LN2 was determined with a designated thermometer. Instead of 77.14 K of pure LN2 a temperature of 77.89 K was determined and used for the calibration procedure.

The sun/sky/lunar CIMEL photometer could only operate as soon as the moon was above the horizon, visible for the photometer from its location on the foredeck container, and the sky was free of clouds. Unfortunately, these measurements were only possible for a 3-4 days in total during Leg 1.

The pyranometer and pyrgeometer were installed on the bow-crane. This location seemed the most favorable to avoid shading by the ships superstructure.

In addition to the technical setup and maintenance of the OCEANET instrumentation an automatic profile retrieval algorithm for Polly-XT (Picasso) was operated to observe online data and aerosol profiles. This automatic dataset will be reanalyzed later according to PollyNET standards (Baars et al., 2016).

One of the main goals of this project is to link the aerosol information to cloud structure and radiative effects. For this purpose, we could make use of the preliminary data from the ARM KAZR cloud radar, the regular radiosoundings on board, and from the OCEANET lidar and microwave radiometer data and implement the Cloudnet algorithms (Illingworth et al., 2007). In this way, synergistic products could already be derived shortly after the measurements which can be accessed online within *Polarstern's* internal network.

Preliminary (expected) results

During PS122/1 several faint aerosol layers up to heights of 14 km were observed with the multi-wavelength Raman Lidar Polly-XT. For example, Figure 3.3.2 shows the 1064-nm range-corrected lidar signal during one of the first cloud-free observation periods. Besides backscattering from aerosols closer to the ground up to 2 km height there were several

stratified layers visible especially at 4-6 and 11-13 km height. The uppermost layer was visible in all cloud-free profiles during the entire Leg 1. Further in-depth analysis of the optical properties is required, but from first analysis it can be stated, that these are most likely highly absorbing pollution aerosols either from the long-ongoing Arctic fires in 2019 or from mid-latitude continental sources.

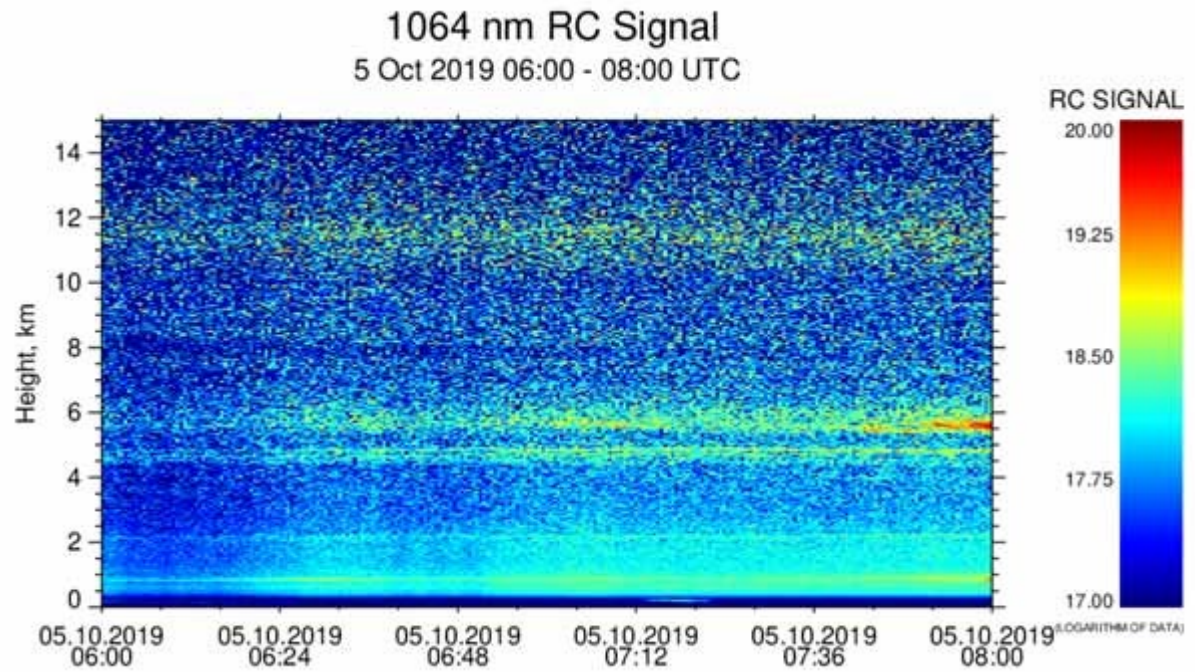

Fig.3.3.2: Range-corrected lidar signal at 1064 nm on 5 October. The signal attenuation right after 0600 UTC was caused by low-level fog or blowing ice crystals near the surface.

The lidar Polly-XT is also equipped with a Raman channel for the detection of water vapor. In a combination with the temperature profiles from the regular *Polarstern* radiosoundings it was possible to derive profiles of relative humidity on a few-minutes resolution on the assumption that the variability of the water vapor drives the relative humidity while the temperature profiles in greater altitudes changes much slower (Guangyao et al., 2018). Such profiles like presented in Figure 3.3.3 for early 2 December 2019 will be a good additional source for in-depth cloud analysis later on.

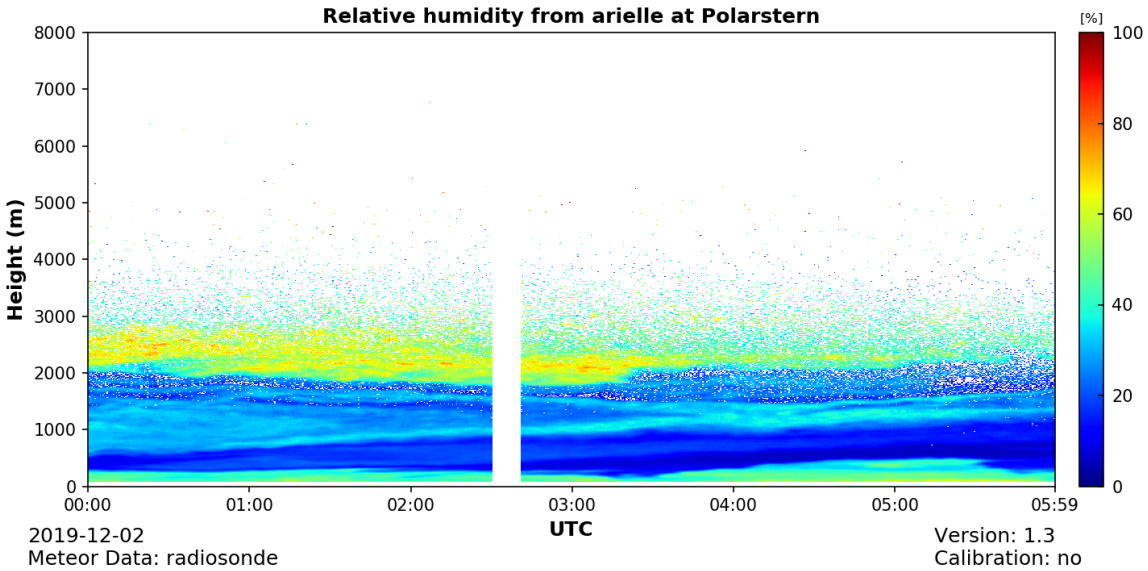

Fig.3.3.3: Relative humidity derived from Polly-XT with the assumption of a constant temperature profile from the 6-h radiosonde.

Additional to the lidar, the OCEANET platform also operated two microwave radiometers, one HATPRO from TROPOS and one LHUMPRO from the University of Cologne. The latter one measures at higher frequencies at which the water-vapor absorption coefficients are stronger, so that it can give better estimates for integrated water vapor and liquid-water path for thin Arctic stratus clouds. For denser cloud systems however, the signals will saturate quickly. Therefore, we employed the combination of both systems to be able to give a full time series of IVW and LWP.

For the first time in the Central Arctic winter we operated a shipborne AERONET sun/sky/lunar Cimel Photometer from the University of Lille. Figure 3.3.4 shows the very first analysis of the Aerosol Optical Depth (AOD) on 11 November at eight different wavelengths.

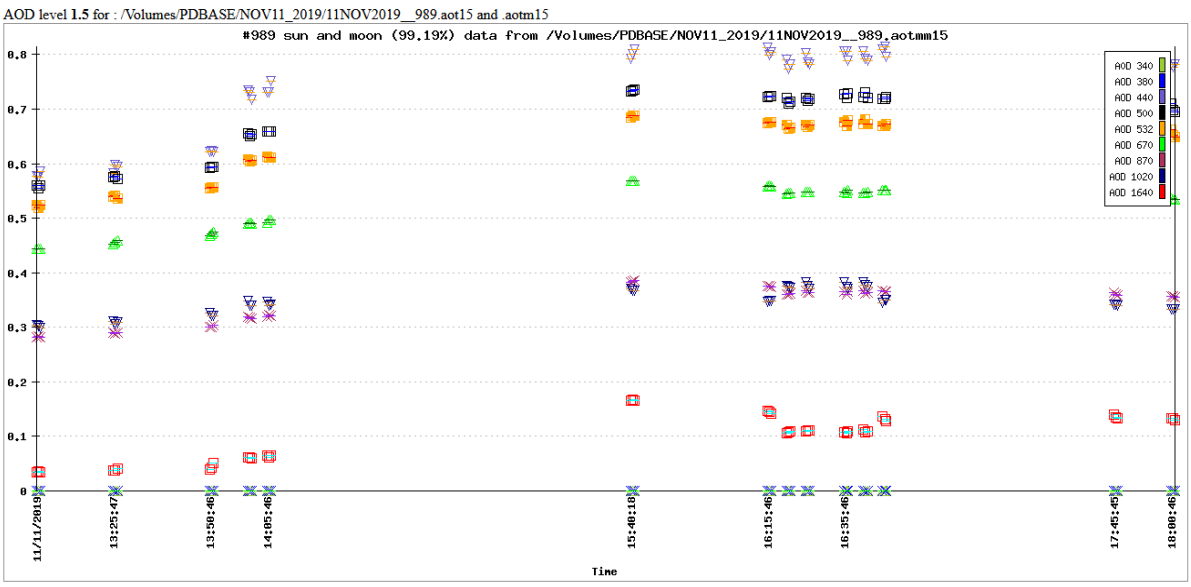

Fig.3.3.4: First preliminary data from the shipborne Lunar Photometer at the Central Arctic. Aerosol Optical Depth vs. time on 11 November 2019.

For MOSAiC we implemented the *Cloudnet* software package at the server system of the OCEANET platform and integrated the preliminary ARM KAZR data (section 3.2), together with the regular 6h radiosounding program (section 3.1), and the Polly-XT lidar to derive synergistic products. Figure 3.3.5 shows an example of the target classification product, and the ice-particle effective radius from this integrated dataset.

During Leg 1 we often observed either pure ice clouds which occasionally contained liquid-water patches or liquid stratus (e.g. from 16 – 18 UTC in Figure 3.3.5) that immediately started nucleation of ice particles and formed ice-particle virgae. The purpose of this early stage of synergistic retrieval was to be able to lively track the current atmospheric observations. Careful post- and reprocessing of these datasets are however needed, once the data went through their individual QA/QC and publication routines.

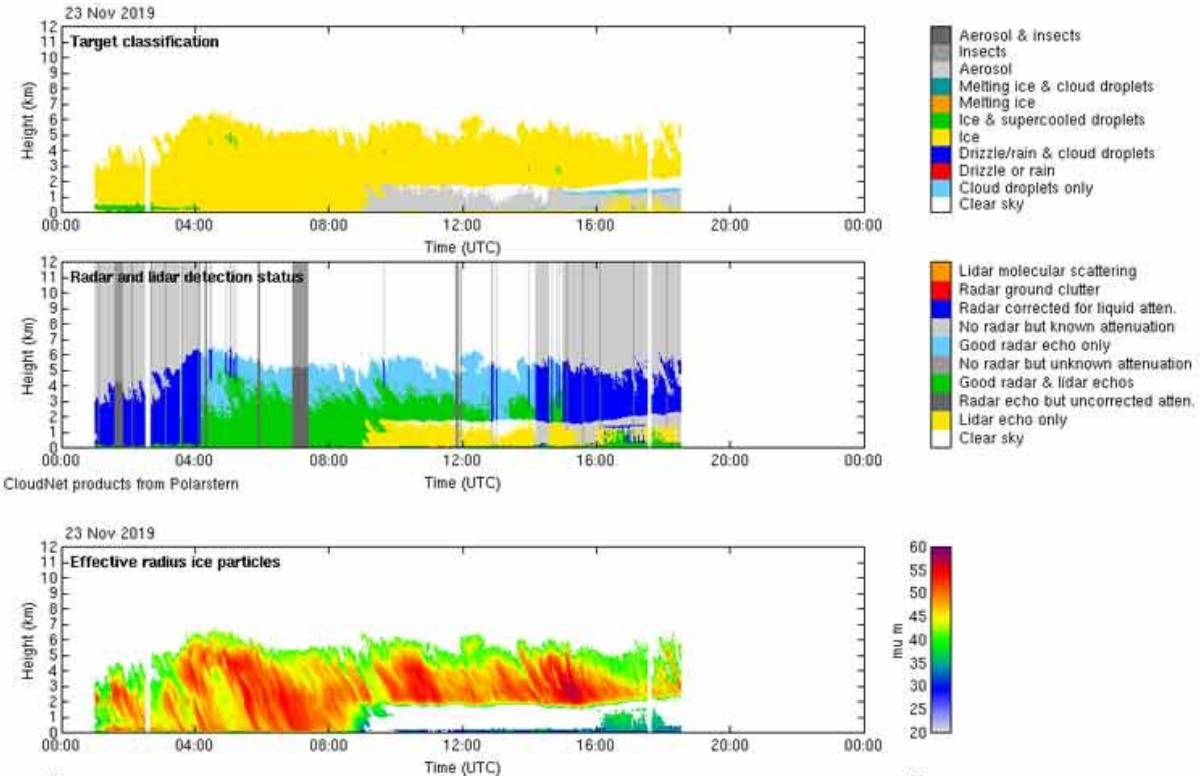

Fig.3.3.5: Some selected Cloudnet products (target classification, detection status, and effective radius of ice particles) automatically generated during Leg 1 on 23 November 2019.

Data management

All data are handled, documented, archived and published following the MOSAiC data policy (see APPENDIX). The raw data from the OCEANET platform are stored in the MCS following the MOSAiC data policy. The Polly-XT lidar data and quicklooks will be processed and made available through PollyNET (http://polly.tropos.de). After final processing the other individual datasets will be published within the PANGAEA data repository (World Data Center PANGAEA Data Publisher for Earth & Environmental Science (www.pangaea.de)).

References

Baars H et al. (2016) An overview of the first decade of PollyNET: an emerging network of automated Raman-polarization lidars for continuous aerosol profiling, Atmos. Chem. Phys., 16, 5111–5137.

Bohlmann S et al. (2018) Ship-borne aerosol profiling with lidar over the Atlantic Ocean: from pure marine conditions to complex dust–smoke mixtures, Atmos. Chem. Phys., 18, 9661–9679.

Engelmann R et al. (2016) The automated multiwavelength Raman polarization and water-vapor lidar PollyXT: the neXT generation, Atmos. Meas. Tech., 9, 1767–1784.

Guangyao D et al. (2018) Calibration of Raman lidar water vapor profiles by means of AERONET photometer observations and GDAS meteorological data. Atmos. Meas. Tech., 11, 2735-2748.

Illingworth AJ et al. (2007) CloudNet: Continuous evaluations of cloud profiles in seven operational models using ground-based observations. Bull. Amer. Meteor. Soc., 88, 883-898.

Kanitz T et al. (2013) North-south cross sections of the vertical aerosol distribution over the Atlantic Ocean from multiwavelength Raman/polarization lidar during *Polarstern* cruises. J. Geophys. Res. Atmos., 118, 2643-2655.

Kanitz T et al. (2011) Contrasting the impact of aerosols at northern and southern midlatitudes on heterogeneous ice formation. Geophys. Res. Lett., 38, L17802.

Yin Z et al. (2019) Aerosol measurements with shipborne sun-sky-lunar photometer and collocated multiwavelength Raman polarization lidar over the Atlantic Ocean. Atmos. Meas. Tech., in press.

3.4 Atmospheric surface fluxes for understanding sea-ice thermodynamics and dynamics

Matthew Shupe[1,2], Ola Persson[1,2], David Costa[1,2], Ian Brooks[3]

(not on board:) Thomas Ayers[2], Christopher Cox[2], Christopher Fairall[2], Michael Gallagher[1,2], Daniel Gottas[2], Jesse Leach[2], Sara Morris[2], Jackson Osborn[1,2], Sergio Pezoa[2], Taneil Uttal[2], Jennifer Hutchings[4], Don Perovich[5], Timothy Stanton[6], Roberta Pirazzini[7]

[1]EDU.CU
[2]GOV.NOAA
[3]UK.UNI-LEEDS
[4]EDU.ORSU
[5]EDU.DARTMOUTH
[6]EDU.NPS
[7]FI.FMI

Objectives

This project aims to examine in detail the interplay of sea-ice thermodynamic and dynamic processes and how these control the state of the ice over a full year, with specific focus here on the atmospheric contributions. In support of this overall goal, project objectives include:

(a) Build comprehensive sea ice energy, upper ocean heat, and sea-ice momentum budgets; examine how these co-vary in space and time over all seasons of the year; and develop temporally-evolving process relationships among multiple key parameters.

(b) Use detailed field observations and a coupled regional model to examine how energy transfer processes (thermodynamics) are influenced by sea-ice deformation (dynamics) on sub-seasonal to seasonal time scales.

(c) Assess sea-ice predictability related to dynamic and thermodynamic process relationships, using a full year of quasi-operational, 10-day sea-ice forecasts.

In support of the broad project goals, the key objective for MOSAiC Leg 1 was to deploy surface flux measurement systems in a way that will enable robust collection of data for a full annual cycle. The parent project includes activities falling within the MOSAiC ATMOS, OCEAN, and ICE teams, and is interdisciplinary in nature. The ATMOS components will be primarily described here, with reference to the other components for context. Further information on OCEAN and ICE components is available in the sections describing the work from those teams at MOSAiC. Links to other ATMOS projects during Leg 1 are also highlighted where appropriate. For example, there are strong links to the ARM, Brooks, Blomquist, and Frey projects (sections 3.2, 3.5, 3.6, 3.8, respectively). Lastly, this report serves as the only summary of the Pirazzini-FMI activity, with a goal of measuring all components of the surface radiation budget over representative ice cover. The atmospheric flux team has worked to support this project while project participants will not be involved in MOSAiC until later legs.

This project is funded by the US National Science Foundation and the US National Oceanic and Atmospheric Administration.

Work at sea

Work during MOSAiC Leg 1 focused on installation of key equipment for measuring surface fluxes of heat and momentum at the atmosphere-ice interface both within the Central Observatory and across the Distributed Network.

Central Observatory. The centerpiece of the installation is the suite of interdisciplinary instruments deployed at Met City, which was initially about 500m distant from *Polarstern*. One primary consideration for the installation of Met City and the heat and momentum flux measurements was to have these as the furthest installation from *Polarstern* with most other activities in the MOSAiC Central Observatory being installed in an approximately linear arrangement back in the direction of *Polarstern*. This installation plan was conceived to minimize the wind sector that would be adversely impacted by other installations and to have a measurement footprint that is as representative as possible of the regional ice conditions. To achieve this objective, the installation was made near the outer wall of the Fortress, capitalizing on the thick, ridged ice in that area for stability, but with many of the specific installations reaching out into the relatively thinner ice just outside the heavily ridged area.

The primary Met City installations for this project include an 11-m meteorological tower (provided by the University of Colorado) and a 30-m meteorological mast (provided by the University of Leeds) to measure key terms related to surface heat and momentum fluxes. Both towers were installed within about 75m of the Met Hut on ice that was not formerly a melt pond, and typically around 1m in thickness. Both tower installations were, however, generally surrounded by regions of ~30cm ice that were former melt ponds. Collectively these two towers have 4 primary measurement levels, allowing observations through the surface layer and into the atmospheric boundary layer. Vaisala T/RH sensors and Metek heated sonic anemometers were installed at nominally 2-, 6-, and 11-m on the tower and at 30-m on the mast. Along with these sensors, a Licor fast water vapor and carbon dioxide sampler was installed adjacent to the 2-m sonic, and an infrared (surface) thermometer, sonic snow depth device, and GPS system were also installed at the 2m height. Two surface flux plates were installed at the ice-snow interface adjacent to the tower, one being underneath the surface temperature and snow depth measurement location. Additional tower-based measurements include, a CLASP, for measuring aerosol size distributions was installed at about 3m height, while two snow particle counters (SPCs) were installed at about 0.5 and 10-m heights (both are part of the Frey project). Data from all of these instruments is logged locally at the base of the 11-m tower and data is transferred automatically to central servers on *Polarstern* via the fiber optic network connection to Met City.

Other key collaborative measurements at Met City include broadband up- and down-welling shortwave and longwave radiation measured by the ARM program (see section 3.2), wind-profiling lidar and sodar (see section 3.5), routine measurements of gas fluxes from an inlet on the 11-m tower (see section 3.6), a Seasonal Ice Mass Balance buoy (SIMB, D. Perovich, Darthmouth University) and an Autonomous Ocean Flux Buoy (AOFB) and pycnocline spar (T. Stanton, San Jose State University). Additionally, this project was responsible for installing a set of broadband up- and downwelling shortwave and longwave radiation measurements from a project led by the Finnish Meteorological Institution (R. Pirazzini) whos participants will not be at MOSAiC until later Legs.

Data collection from the flux tower was started while it was laying down, providing an intercomparison data set between all instruments at the same height from approximately 15 October until they were lifted up to their installed height on 24 October. Data loss for most systems was limited to primarily the times of line power loss from *Polarstern* due to ice movements on 17-28 November. Tower data recovery during this time period was about 70% due to operations on generators. During the rest of the period, data recovery was about 98%,

leading to an overall recovery of 91% of data from the 11-m tower during Leg 1. The 30-m mast was installed at its full height on 26 October, but collapsed due to ice movements on 18 November. It was thereafter re-installed at a nominal height of 23m on 9 December. Due to the long period of no operations on this mast, data recovery during Leg 1 was only about 53%.

Regarding the wind sectors, the measurement angles from about 40-110 degrees are potentially affected by artificial surface roughness elements such as the Remote Sensing City (RS), Ocean City (OC), Balloon Town (TB), and the *Polarstern* itself. Wind directions from W-NW through NE come from the rough ice inside the Fortress, with complex ridges up to 4m height. While sampling sites also exist in this area, they likely do not significantly alter the turbulent fluxes from these wind directions because of the naturally rough ice in the area. From the W-NW through S to E-SE wind directions, the ice in the first month of the drift was fairly smooth and relatively thin (30-50cm). During the week of 16-22 November, episodic rapid ice movement changed the configuration of the Central Observatory, moving Met City towards the forward of *Polarstern* at a range of about 400m (Figure 3.4.1). This change increased the size of the wind sector that includes potential artificial roughness elements. After this transition, the ship occupied the 0-50 degree wind sector.

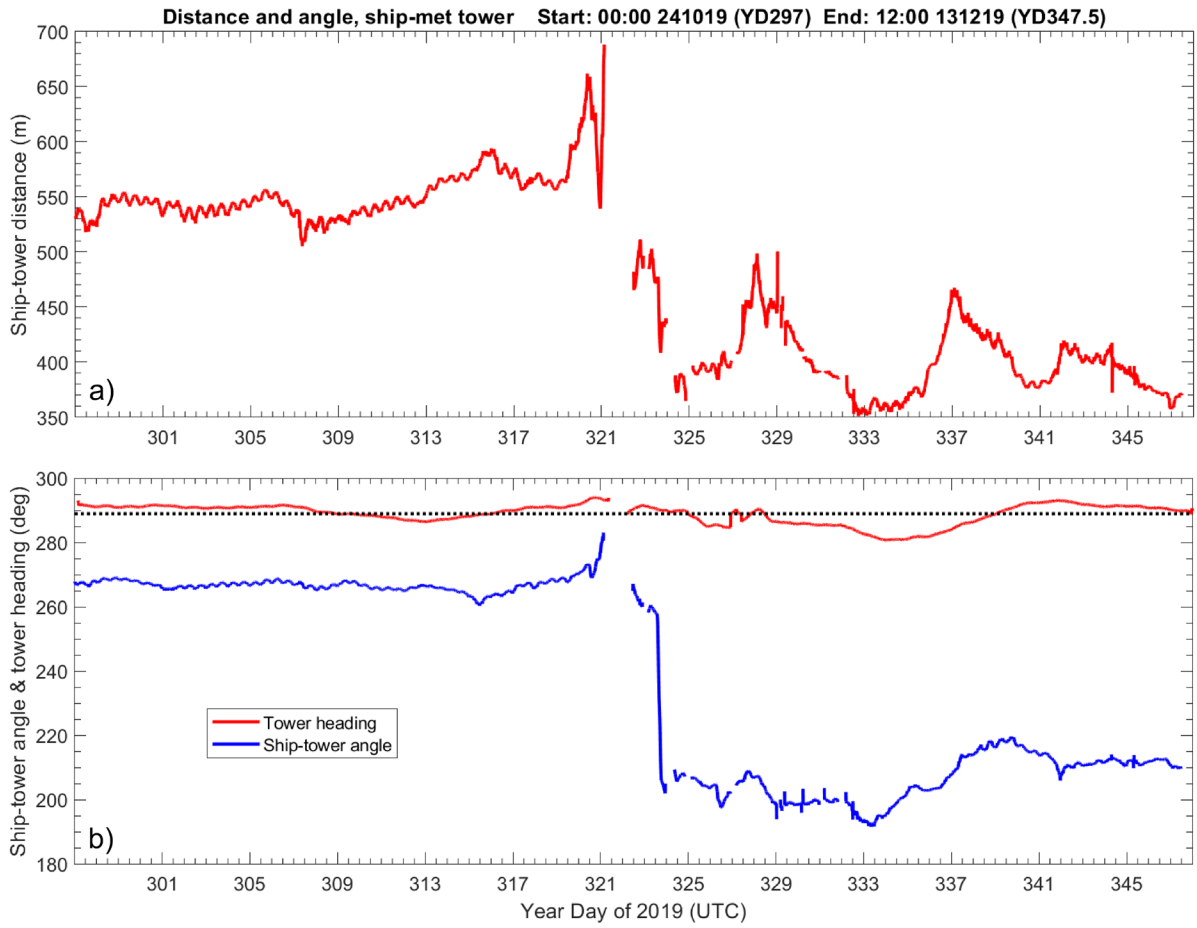

Fig.3.4.6: a) Distance and b) angle (blue) between the ship GPS and the Met City tower GPS as a function of time during Leg 1. In b) the heading given by the Met City tower GPS (red) shows only slight rotation of the tower floe during Leg 1 despite significant movements.

Distributed Network. To understand the variability of surface heat and momentum fluxes over a broader domain and including more local conditions, similar measurements to those described above were made within the MOSAiC Distributed Network. These distributed observations also allow for the possibility to calculate atmospheric stress divergence which

can be linked to ice divergence across the MOSAiC network. Installation of Atmospheric Surface Flux Stations (ASFS) at the three L sites in the first two weeks of October was done via the *Akademik Fedorov* cruise as part of MOSAiC Leg 1a and is documented in the appropriate cruise report for that activity. In short, the L sites were installed in an approximate triangular shape around *Polarstern* with distances to the individual sites ranging from 12 to 23 km. The ASFS are similar to the meteorological tower and other installations made at Met City, although with a single level of measurements. Instruments include one sonic anemometer, Vaisala temperature, pressure, and relative humidity measurements, a Licor sensor for measuring fast water vapor (which was not always turned on), a sonic snow depth sensor, an infrared (surface) thermometer, a GPS system, two cameras, and a set of up- and down-welling longwave and shortwave radiometers. This full suite of observations is supported for semi-autonomous operations by a methanol fuel cell with battery power storage and dual communication with *Polarstern* using line-of-site radio and Iridium communications. Adjacent to the ASFS at the three L sites were installations of the SIMB and AOFB that were also installed at the Central Observatory. Additionally, a full network of GPS position buoys was installed by a key project collaborator (J. Hutchings, Oregon State University) across the MOSAiC distributed network to allow for explicit linkages between the thermodynamic and dynamic influences on sea ice.

During Leg 1 the ASFS stations at the L-sites were visited via helicopter at least once per month for basic station maintenance, including cleaning instruments, resupplying the fuel, and extracting the full-resolution data. Table 3.4.1 shows the specific site visits and provides a brief summary of site activities during those visits. The ASFS had a couple of significant issues during Leg 1. The power system on the L1 station failed and had to be replaced on 10 November. Later on that same day, the L2 station was damaged by a polar bear, requiring a major rebuilding effort that was completed on 30 November. All other visits have been for routine maintenance or minor adjustments to operations.

Tab.3.4.1: L-site visit Summary

Site	Date	Summary of Activities
L1 – ASFS40 (12 km @ 220°)	5 Oct	Site installation
	15 Oct	Maintenance, Remove Licor from operation
	10 Nov	Maintenance, Change power system
	7 Dec	Maintenance
L2 – ASFS30 (13.2 km @ 128°)	7 Oct	Site installation
	16 Oct	Maintenance, Remove Licor from operation
	6 Nov	Maintenance, Fix radiometer ventilator
	14 Nov	Assessment of damage, Remove power system
	22 Nov	Remove additional damage equipment, Install new sonic
	30 Nov	Install power system, Install other instrument fixes
	6 Dec	Final instrument fixes
L3 – ASFS50 (23 km @ 357°)	10 Oct	Site installation
	14 Nov	Maintenance
	6 Dec	Maintenance, Change meteorological instrument

Preliminary (expected) results

Measurements made as part of this project have provided up to 2 months of high-quality estimates of atmospheric surface heat and momentum fluxes at four locations across the MOSAiC domain, as well as detailed lower atmospheric structure at the MOSAiC ice camp.

These fluxes will be combined with project partner measurements of ocean heat fluxes, sea ice thermodynamic state and thickness, and regional-scale sea-ice movement and deformation to understand the dynamic and thermodynamic drivers of the sea-ice life cycle.

During Leg 1, heat loss was observed from the snow/ice surface to the atmosphere during this autumn time period. The conductive heat loss within the ice from the ocean to the atmosphere includes a contribution of turbulent heat flux from the ocean to the ice bottom and the heat loss given off during the freezing of sea water forming new ice at the ice bottom. The combined net radiative and turbulent heat flux at the air-snow interface represents the transfer of this heat to the atmosphere. The combined atmospheric and ocean heat fluxes will be calculated from the flux tower, ARM radiation, and AOFB data acquired at Met City. The conductive flux within the snow near the ice/snow interface and from the bottom of the ice is, to a first order, represented by the measurements from the two flux plates near the flux tower (Figure 3.4.2c), and should be consistent with the temperature structure observed through the ice by the collocated SIMB system. These values are positive most of the time, with observed values up to 50 W m^{-2}, though they can become negative during warm-air advection events, as during the pre-storm low-level jet on 16 November. The conductive flux is dependent on thickness of the ice and snow cover and on the near-surface air temperature. Two of these three dependencies can be seen in Figure 3.4.2 at the flux tower. The sign of the atmosphere-surface turbulent heat fluxes depends on the vertical gradient of surface-layer temperature, with a negative gradient producing surface heat loss to the atmosphere while a positive gradient (temperature inversion) means that the atmospheric turbulent fluxes are warming the surface. Vertical gradients across the tower show that both signs occur, though in the mean a temperature inversion exists. Hence, turbulent heat fluxes have generally warmed the ice during Leg 1. The primary mechanism for the loss of the heat conducted from the ocean through the ice and snow to the atmosphere is expected to be through longwave radiation. The measurements for the direct calculations of the turbulent and radiative heat fluxes were obtained at Met City during Leg 1 and will continue.

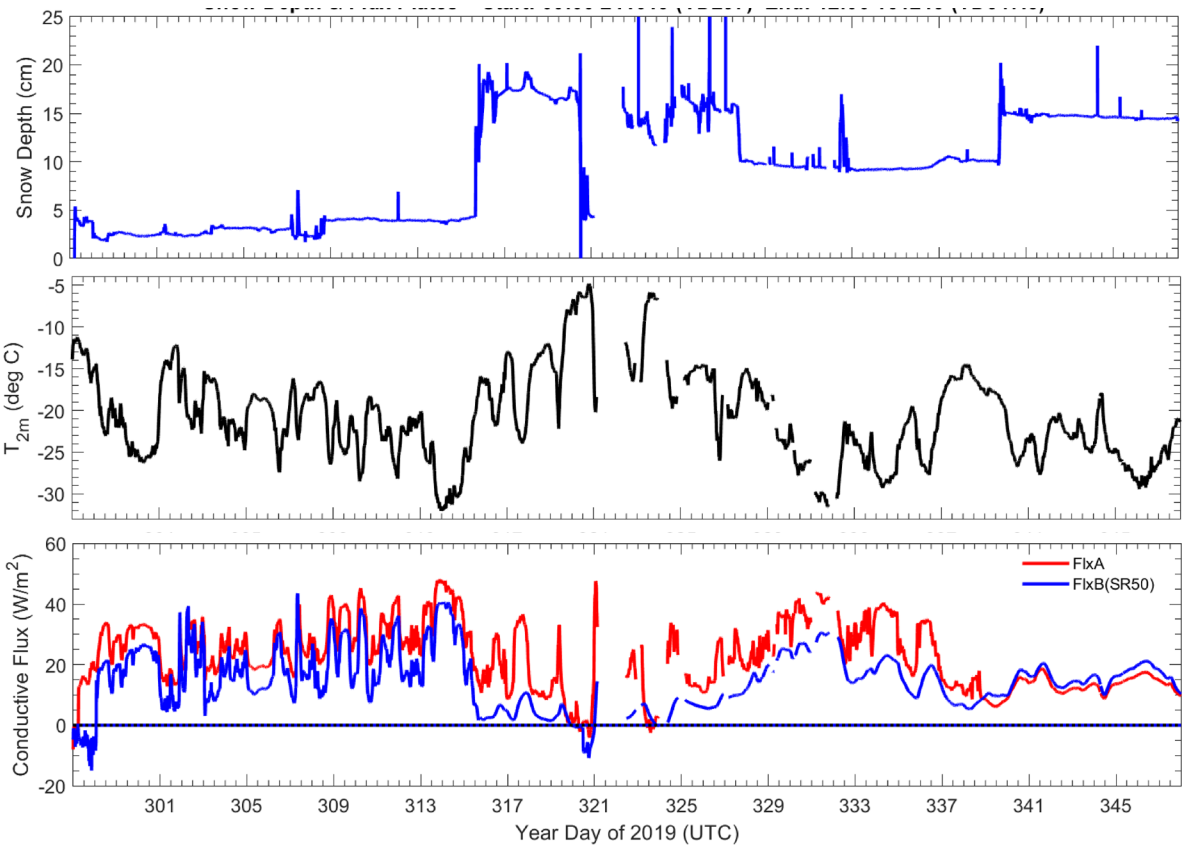

Fig.3.4.7: Timeseries of a) SR50 snow depth above Flux Plate B near the Met City tower, b) the 2-m temperature, and c) the conductive flux as measured by Flux plates A (red) and B (blue). Flux plate A was initially positioned over relatively thin ice (~40 cm) while Flux B was over thicker ice (~ 1 m). The snow-cover evolution in a) is primarily driven by movement of a snow drift and hence mainly relevant for Flux plate B, which was co-located. The snow thickness curve requires editing, as many of the spikes are likely effects of blowing snow or power outages.

We also expect that atmospheric features passing over the distributed network site reveal their motion characteristics (e.g., phase velocities) and spatial impact variations. Since ice conditions are different at the different L sites (and Met City), we expect quantitatively different balances between the various components of the surface energy budget depending on the ice and snow characteristics at each site (e.g., Figure 3.4.3a). Understanding this type of variability across the MOSAiC domain will be important for any attempts to "upscale" and generalize the MOSAiC results. Spatial variations in winds and radiation (e.g., Figures 3.4.3b, c) will support the diagnosis of frontal features, such as atmospheric divergence or deformation, and movements of cloud boundaries. Spatio-temporal variations in high-frequency pressure measurements may even allow for the diagnosis of gravity wave features that may be common in this generally stable atmospheric boundary layer, and may impact turbulent heat and momentum fluxes and even boundary-layer clouds.

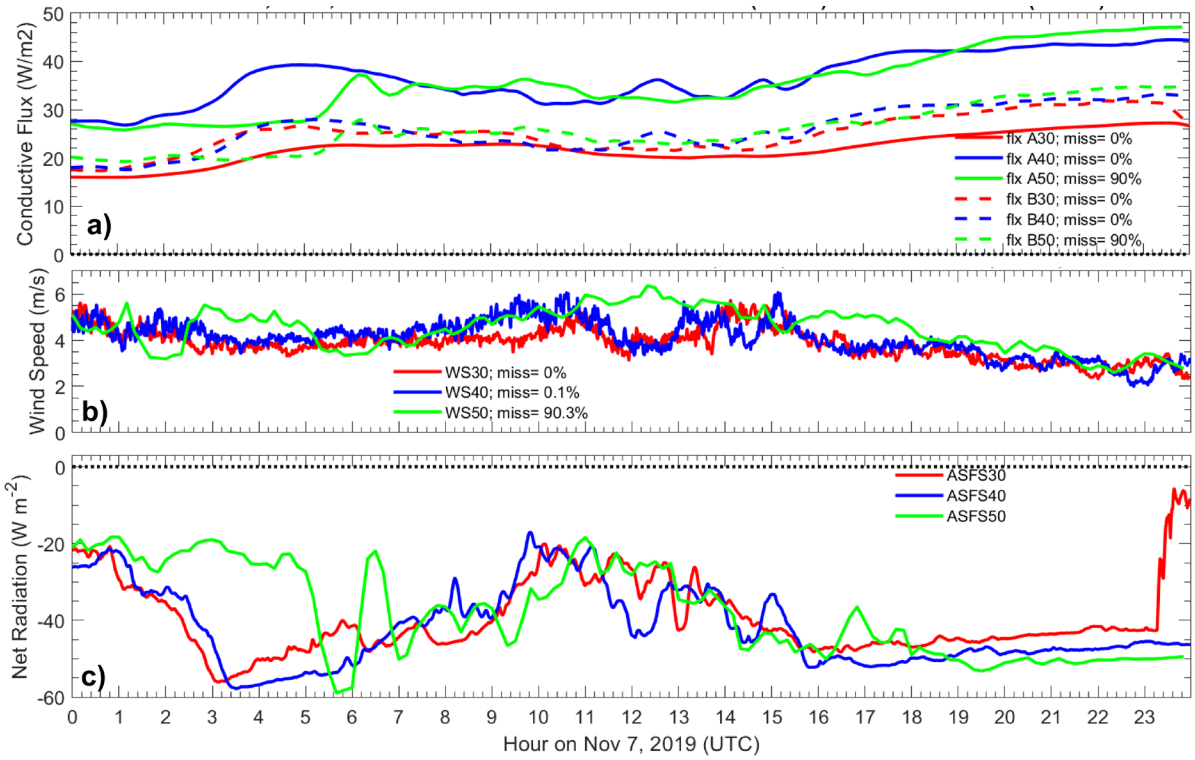

Fig.3.4.8: Example time series of a) conductive heat flux, b) wind speed, and c) net radiation from the sites L1 (ASFS40, blue), L2 (ASFS30, red) and L3 (ASFS50, green) on 7 November 2019. Data for sites L1 and L2 are 1-min averages, while that for L3 is 10-min averages.

In the future, the data produced during Leg 1 will be widely used for research examining surface energy budget processes, atmospheric stability, turbulent exchange of various parameters, and other topics. Relationships among different components of the atmospheric surface energy budget, as well as the energy budgets of the ice and upper ocean, will be developed and explored. The data will also be used to assess quasi-operational 10-day model forecasts from the regional Coupled Arctic Forecast System (CAFS) to evaluate the processes responsible for forecast skill for short versus medium-range forecasts.

Data management

Data produced at the Met City installation are archived locally in Met City and duplicated in the flux laboratory container onboard *Polarstern*. Data produced at the remote ASFS sites are archived locally on the remote systems; some sub-set of this data is transferred to *Polarstern* via a combination of radio or Iridium modems. The full set of ASFS site data is transferred to *Polarstern* after routine site visits. All data is redundantly archived on the server in the flux laboratory container onboard *Polarstern*. Additionally, a copy of all raw data has been uploaded to the MOSAiC Central Storage onboard *Polarstern*; this data has not yet undergone detailed quality assurance and calibration. Long term archival of quality-controlled data will be done on PANGAEA (World Data Center PANGAEA Data Publisher for Earth & Environmental Science (www.pangaea.de)) and/or on the Arctic Data Center archive, according to the protocol agreed upon between these two archives. All data are handled, documented, archived and published following the MOSAiC data policy. Exceptions will to be documented in written agreements between the data provider and the MOSAiC Project Board and data manager.

References

No references

3.5 Boundary Layer Dynamics

Ian Brooks[1], Andreas Preußer[2] [1]UK.UNI-LEEDS
(not on board:) Ryan Neely III[1], Barbara Brooks[1], Günther Heinemann[2] [2]DE.UNITRIER

Objectives

The overarching goal is to develop a new understanding of the physical processes governing atmospheric boundary layer structure, turbulent mixing, and the interactions with both the surface and cloud in the central Arctic.

Our specific objectives are to:

- Characterize the turbulent dynamics of the Arctic atmospheric boundary layer and the physical processes controlling it over a full annual cycle. BL mixing directly affects the surface heat flux and both influences cloud properties and is influenced by in-cloud processes, and thus impacts the radiative fluxes and surface energy budget, contributing to ice formation/melt.
- Determine the interactions of Arctic boundary layer structure with the surface turbulent fluxes of momentum and heat. Surface fluxes are a controlling influence on lower BL structure. Elevated sources of turbulence, e.g. wind speed jets and radiative cooling at cloud top, dominate the control of upper BL structure and can impact surface fluxes where surface forcing of turbulence is weak, and thus the surface energy budget and ice evolution.
- Identify and describe the significant processes controlling coupling/decoupling of BL cloud to the surface. Decoupling isolates BL cloud from surface sources of moisture and aerosol; this may affect cloud properties (iii) and thus the surface radiation budget.

Work at sea

The boundary-layer dynamics measurements were obtained via active remote sensing using: 3 Doppler lidars and a phased array Doppler sodar.

Two lidars were installed on board *Polarstern* on P-deck: A Halo Photonics Streamline lidar from the University of Trier, and a Galion G4000 wind profiling lidar. A second Halo Streamline lidar was installed at the *Met City* site on the pack ice along with a Scintec MFAS sodar. The lidars all operate at near infrared wavelengths, and rely on reflected light from particles in the atmosphere (aerosols, cloud droplets, and ice crystals) to make a measurement. The Halo lidars provide measurements of backscatter intensity and along-beam Doppler velocity while the Galion provides only Doppler velocity as an output.

The Galion lidar was configured to make continuous VAD (Velocity Azimuth Display) scans from which vertical profiles of wind speed and direction can be derived with a time resolution of approximately 2.5 minutes and a vertical resolution of 20m.

The Halo lidars were initially configured to work in a synchronized mode to make measurements of the same volume of air from two different directions in a ‘virtual tower’. This allows the air motion to be resolved in 2-dimensions. The virtual tower also provides 2 intersecting RHI (range height indicator) scans which can be used to derive estimates of turbulent velocity variances and turbulent kinetic energy profiles (Banta et al. 2006). In order to calculate the scan configurations for each lidar required for the synchronized measurements accurate relative positions and orientations of the two instruments is required. During the course of leg 1, repeated movement of the ice made it difficult to maintain the synchronized scans and it was clear that the instrument caretakers for legs 2,4,5, and 6, where no one from Leeds or Trier was on board would be unable to do so. The decision was made late in the leg

to configure the two systems to operate independently, each conducting a set of RHI scans at multiple azimuth angles, maximizing the information on boundary layer turbulent structure while minimizing the effort required by the instrument caretakers.

The sodar uses acoustic backscatter to make its measurement. A sequence of audible acoustic pulses is transmitted. Echoes are returned from density gradients in the atmosphere – these arise primarily at gradients in temperature, either large scale gradients such as temperature inversions, or small scale gradients resulting from turbulence. The intensity of the acoustic backscatter provides some information on the turbulent and thermodynamic structure of the lower atmosphere. The Doppler shift of the echo provides a measurement of air motion. The acoustic beam can be steered off the vertical, allowing measurements of horizontal wind components to be made giving another measurement of the wind profile. The sodar vertical resolution is 10m, with a range from 40-1000m (though the upper limit is strongly dependent upon conditions and rarely reaches this absolute maximum). Wind profiles are obtained at 10 minute intervals and vertical backscatter profiles every 5 minutes.

Preliminary (expected) results

Figure 3.5.1 is an example raw acoustic backscatter signal from the sodar on 12 December 2019, showing a deepening mixing layer from about 16:00 onwards. Calibration of the backscatter with the surface sensible heat flux will allow for a temperature structure function to be calculated. This provides a good measure of the extent of the well mixed layer above the surface.

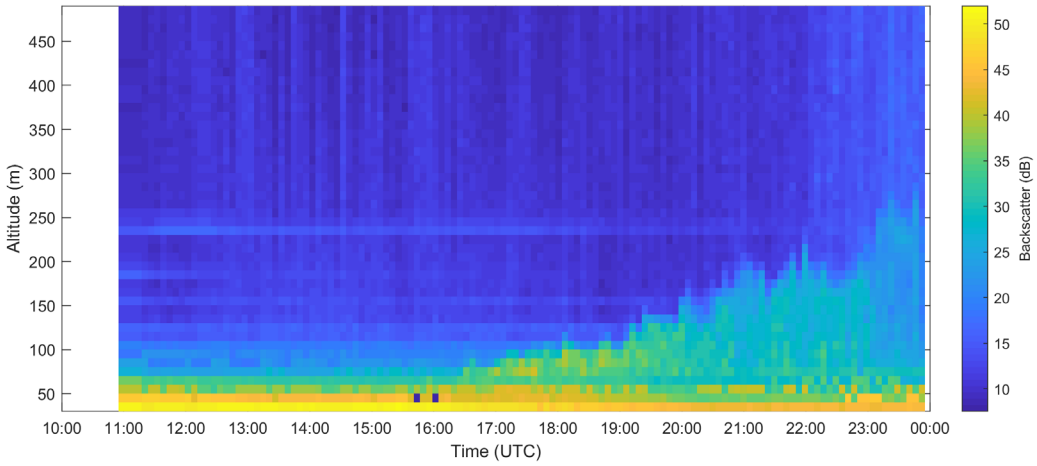

Fig.3.5.1: Sodar backscatter from 12 December 2019.

Figure 3.5.2 shows an example wind speed time-height section from the Galion lidar installed onboard *Polarstern*. A broad low-level wind-speed jet is visible from 09:00-15:00 at around 300 m.

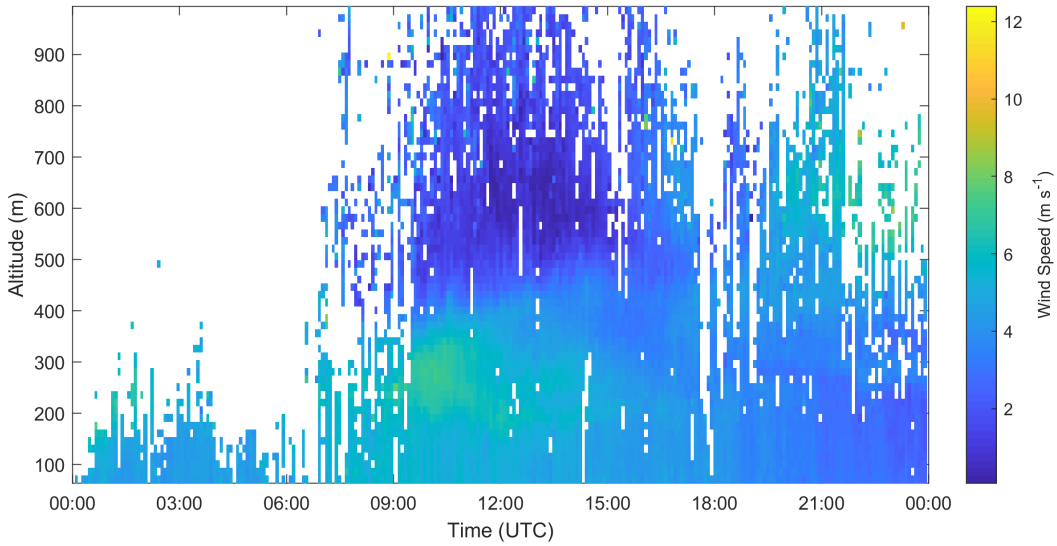

Fig.3.5.2: Profile of wind speeds derived from the Gallion lidar installed on the Polarstern P-deck. Winds can only be estimated where there is enough backscattered atmospheric signal.

Data management

All data are handled, documented, archived and published following the MOSAiC data policy (see APPENDIX). Raw data, including instrument quality control flags, is archived daily on the MOSAiC central Storage system and on a RAID belonging to Leeds. Final data products will be stored at the PANGAEA data repository (World Data Center PANGAEA Data Publisher for Earth & Environmental Science (www.pangaea.de)).

References

Banta RM, Pichugina YL, Brewer WA (2006) Turbulent Velocity-Variance Profiles in the Stable Boundary Layer Generated by a Nocturnal Low-Level Jet, Journal of the Atmospheric Sciences, 63, 2700-2719

3.6 Trace gas flux group

Byron Blomquist[1,2], Steve Archer[3], Jacques Hueber[1]

(not on board:) Detlev Helmig[1], Laurens Ganzeveld[4], Christopher Fairall[2], Dean Howard[1], Ludovich Bariteau[1,2], Kevin Posman[3], Hans-Werner Jacobi[5], Helene Angot[1], Sjoerd Barten[4], William Sturges[6], Lucy Carpenter[7]

[1]EDU.CU
[2]GOV.NOAA
[3]ORG.BIGELOW
[4]NL.WUR
[5]FR.UGA
[6]UK.AC.UEA
[7]UK.AC.YORK

Objectives

The MOSAiC trace gas flux group encompasses a wide range of scientific interests and specializations, with a focus on the air-sea exchange of four primary climate-active trace gases – carbon dioxide (CO_2), methane (CH_4), dimethyl sulfide (DMS) and ozone (O_3) – and a broader interest in the transport, reactivity, surface exchange and chemical atmospheric budgets of volatile organic carbon compounds (VOCs), chlorofluorocarbons (CFCs) and elemental mercury (Hg^0).

There were three measurement objectives for Leg 1: continuous eddy correlation (EC) flux measurements of the four primary gases; continuous mean concentration measurements of an expanded list of trace gases including VOCs, CFCs, nitrogen oxides (NO/NO_2) and Hg^0; and dynamic chamber flux measurements of the primary gases over undisturbed snow and ice, at smaller spatial and temporal scales compared to the eddy correlation fluxes.

Longer term modeling objectives include the development of a physical gas transfer parameterization suitable for the sea ice environment, 1D modeling of the atmospheric surface exchange, vertical transport and reactivity of these gases, and 3D modeling to assess the significance of Central Arctic air-sea transfer in regional and global atmospheric trace gas budgets.

Work at sea

Table 3.6.1 provides a list of the measurement systems deployed for Leg 1 with their location, sampling frequency and SensorWeb short name. These systems are briefly described below.

Tab.3.6.1: Measurement Systems Deployed for Leg 1

Measurement System	Sampling Location	Sample Rate	SensorWeb 'Short Name'
DMS API Mass Spectrometer	ship bow tower	10 Hz continuous	dms_apims_ship_bow
Picarro G2311-f CRDS	ship bow tower	10 Hz continuous	crds_ghg_ship_bow
Chemiluminescent Ozone	ship bow tower	10 Hz continuous	ozone_fast_ship_bow
Metek uSonic-3 Anemometer	ship bow tower	10 Hz continuous	sonic_anemometer_3D_ship_bow
Licor 7500DS	ship bow tower	10 Hz continuous	licor_7500ds_ship_bow
RM Young 86004 Sonic Anemometer	ship bow tower	1 Hz continuous	sonic_anemometer_2D_ship_bow
Chemiluminescent NO/NO2	ship bow crane	10 per minute	nox_ship_bow
TEI model 49C ozone analyzer	ship bow crane	1 per minute	ozone_slow_ship_bow
Tekran 2537B mercury analyzer	ship bow crane	1 per 5-15 minute	hg_ship_bow
Agilent GC Mass Spectrometer	ship bow crane	~15-18 per day	gcms_ship_bow
Picarro G2311-f CRDS	met city 10m tower	10 Hz continuous	crds_ghg_ice_station_tower

Measurement System	Sampling Location	Sample Rate	SensorWeb 'Short Name'
CO2/CH4 Flux Chamber	various	1-2 per deployment	co2_ch4_chamber_portable
Ozone Flux Chamber	various	1-2 per deployment	ozone_chamber_portable
Michell S8000 hygrometer	ship bow tower	~1 per minute	t_rh_ship_bow

Ship EC Fluxes: A Metek uSonic3 USA-1 sonic anemometer is mounted to the top of the met mast on the *Polarstern* bow crane for mean wind and turbulence measurements (Figure 3.6.1a), a Li-COR 7500DS fast CO_2 and water vapor sensor is mounted about 1m below the USA-1 sonic head, and an RM Young model 86004 2D sonic anemometer is ~1m below the LI-COR. Inlet tubes (1/2" teflon) for three fast trace gas analyzers are located just at the base of the Metek sonic, extending down to a laboratory container in the E-deck hold, at position E-10. Inlet tubes are ~42m in length and are insulated and heated to 15-20 °C.

In the E-10 lab van, a Picarro model G2311-f cavity ring-down spectrometer (CRDS) is used for 10 Hz CO_2, CH_4 and water vapor measurements. The Picarro inlet flow rate was set to ~ 50 LPM and the analyzer subsampled from this inlet at ~5 LPM. This type of analyzer has been previously used for CO_2 flux measurements at sea with a sample air dryer (Blomquist et al. 2014). A dryer was installed for MOSAiC but not used since ambient humidity for Leg 1 was very low, with frost points generally less than -20 °C. A fast chemiluminescent ozone analyzer (Bariteau et al. 2010) is used for ozone flux, and an Atmospheric Pressure Ionization Mass Spectrometer (APIMS) for DMS flux (Blomquist et al. 2010). Inlet flow for the APIMS was comparable to the CRDS. The ozone inlet flow was 30 LPM.

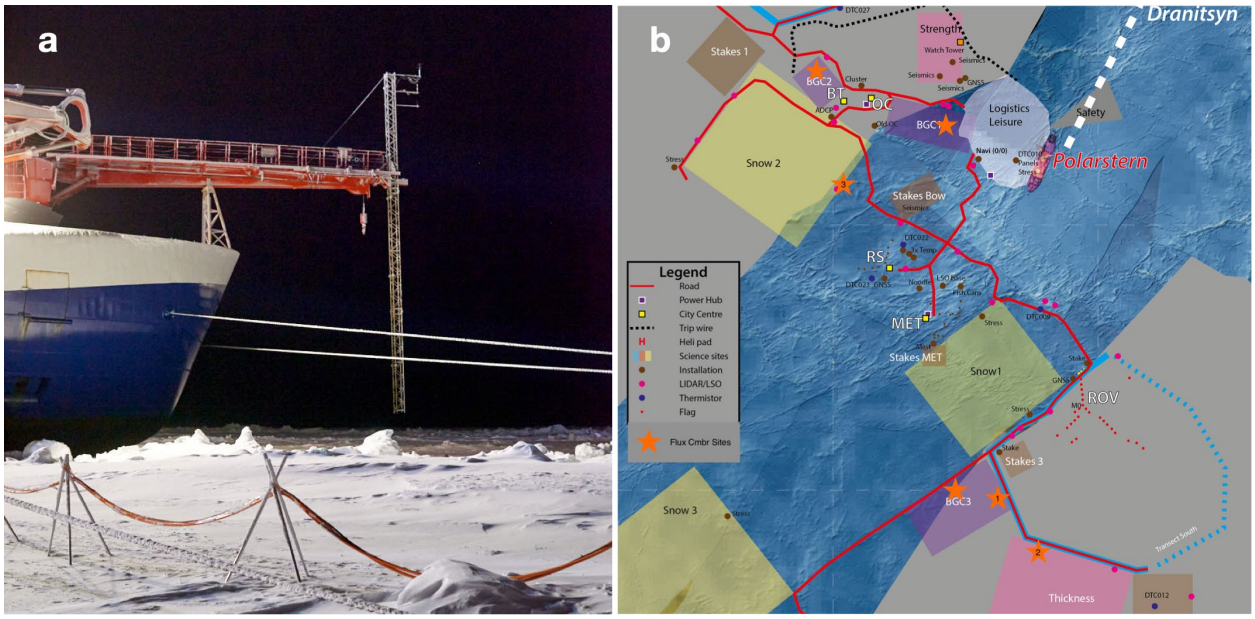

Fig.3.6.1: a) Polarstern bow crane and met tower. b) Site map showing ship, Met City and flux chamber sampling sites during leg 1.

Met City EC Fluxes: Trace gas flux measurements at Met City were conducted in cooperation with the Univ. Colorado CIRES / NOAA flux group (section 3.4) using their 11m flux tower. A heated, insulated air sampling inlet is installed at the top of the tower near the 11m sonic anemometer (Metek uSonic 3). A Picarro model G2311-f CRDS for fast CO_2/CH_4/H_2O measurements, identical to the ship system, is located in the met hut approximately 20m from the tower. Serial data from this analyzer is logged on the CIRES/NOAA acquisition system at the base of the tower. Inlet flow rate and other sampling details were similar to the ship system.

Other Shipboard Trace Gas Measurements: In addition to the flux systems mentioned above, the E-10 lab van contains an Agilent GC Mass Spectrometer (GCMS) system for ambient air VOC and CFC measurements. GCMS sampling is continuous, at about 15-18 samples per day. Table 3.6.2 lists the target compounds for the GCMS analysis. Other instruments in the E-10 van include a chemiluminescent NO/NO_2 analyzer, TEI model 49C ozone analyzer, Michell S8000 chilled-mirror hygrometer, and Tekran 2537B gaseous mercury analyzer. Dedicated sampling lines for these instruments extend up to the ship bow crane near the base of the met tower. These are all fitted with teflon inlet filters (5 uM).

Tab.3.6.2: Target Compounds for GCMS Analysis

Hydrocarbons	Halogenated Cmpds	Other
Ethane	HFC-125	SF_6
Propane	HFC-134a	OCS
Propyne	HFC-152a	CS_2
Acetaldehyde	HFC-22	Dimethylsulfide
iso-Butane	Methyl Chloride	
n-Butane	CFC-12	
Acetone	HCFC-142b	
iso-Pentane	Methyl Bromide	
Isoprene	HCFC-124	
n-Pentane	H-1211	
Benzene	CFC-114	
Toluene	CH_2Cl_2	
	Methyl Iodide	
	HCFC-141b	
	CFC-11	
	CFC-113	
	chloroform	
	CH_2BrCl	

Hydrocarbons	Halogenated Cmpds	Other
	CH_2Br_2	
	CCl_4	
	Perchloroethylene	
	$CHBrCl_2$	
	$CHBr_3$	

NOAA/GMD Sample Flasks: In addition to the *in-situ* trace gas measurements described above, we collected weekly air samples for greenhouse gas analysis by the NOAA Global Monitoring Division. These will be shipped to the NOAA facility in Boulder, Colorado at the end of the cruise leg for analysis.

CO_2 / CH_4 Flux Chamber Measurements: A dynamic chamber system incorporating two high precision gas analyzers (LI-COR LI-7810 CO_2/CH_4/H_2O and LICOR LI-7815 CO_2/H_2O) was deployed several times at a variety of locations during Leg 1 (Figure 3.6.2). This system measures direct emission or deposition of gases at the snow or ice surface with a small footprint (0.343 m^2) over short timescales (<1 hr) and with minimal surface disruption. The intent is to obtain a surface flux measurement that complements the EC fluxes and facilitates an assessment of spatial variability in sea ice gas transfer, closely linking the observed fluxes to environmental controls and physical/biogeochemical factors. A collaborative sampling strategy with ICE, ECO and BGC teams is necessary to achieve this goal.

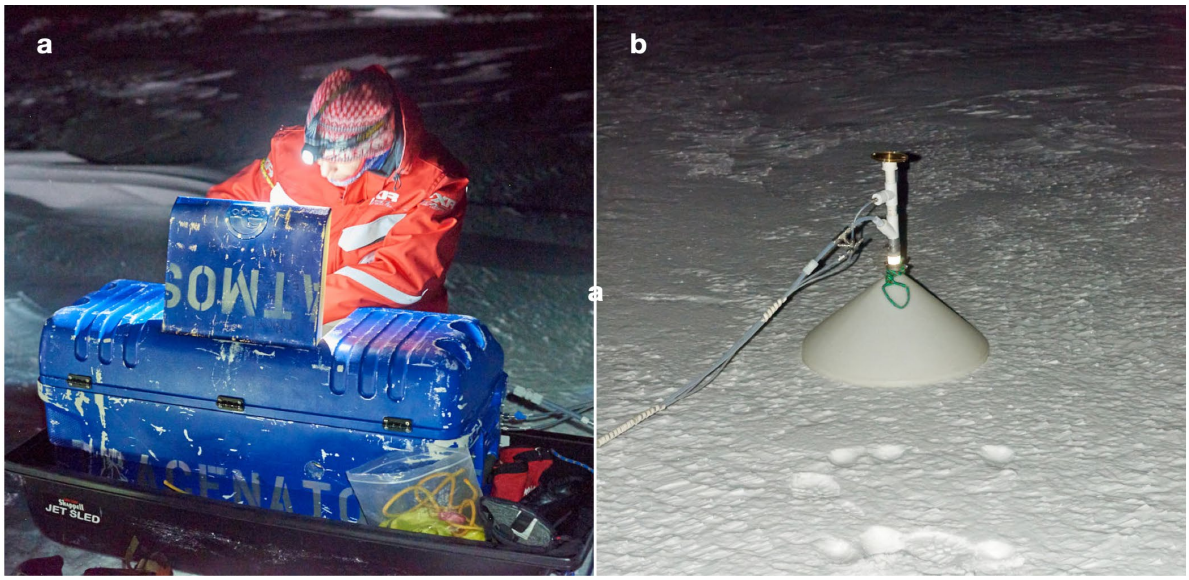

Fig.3.6.2: CO_2/CH_4 dynamic chamber flux system. a) analyzer box. b) flux chamber.

Sampling Site Locations: Figure 3.6.1b shows the relative locations and orientation of Met City and the various chamber flux sites with respect to the ship. We anticipate footprints for EC flux measurements from the ship bow and Met City towers will cover an area including chamber sampling sites #1, #2 and BGC3 when southeasterly to southerly winds prevail.

Preliminary (expected) results

For the ship, valid gas concentration measurements are only possible over a limited 'clean sector' in the relative wind direction. During Leg 1 this is defined as +/- 130° from the bow. In addition, a wind speed lower limit of 1 m/s is applied. To avoid inlet contamination, air sample flow is shut down and the gas inlets are back-flushed with clean air when wind conditions are 'out-of-sector'.

Several gas analyzers are routinely put in standby mode during 'out of sector' conditions, including the Picarro, APIMS, GCMS and mercury analyzers. Thus, there are no data from these systems during 'out-of-sector' wind conditions. Other systems, such as the ozone and NO/NO_2 analyzers, remain running when the inlets are in back flush mode, but only measure laboratory clean air at this time and the data are therefore not useful.

Figure 3.6.3 shows the number of hours of 'good wind' conditions at the ship tower for each day of Leg 1 (top panel). Over 1368 hours of sampling during Leg 1 we have 1004 hours that meet the criteria for good wind conditions defined above. Of these not all will be suitable for turbulent flux measurements, but concentration data should be good, with minimal interference from ship contamination. Other panels in Figures 3.6.3 and 3.6.4 show the number of hours of operation or the number of samples per day for each analyzer.

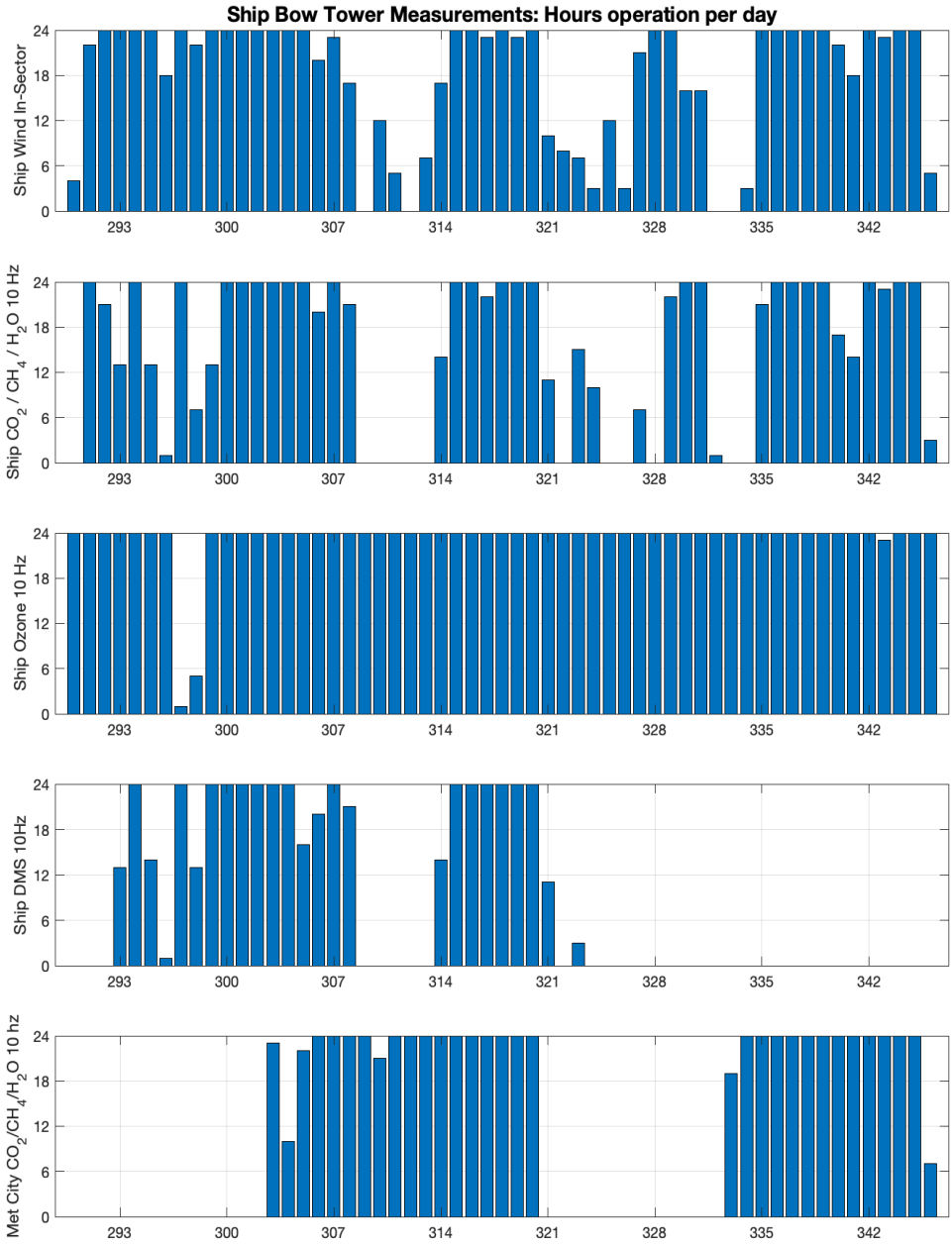

Fig.3.6.3: Ship flux system operations during Leg 1. Top panel: Hours per day when the relative wind direction and speed are "in sector." Second panel: Picarro CRDS flux analyser, daily hours of operation. Third panel: Fast ozone analyser, daily hours of operation. Fourth panel: DMS APIMS, daily hours of operations. Fifth panel: Met City Picarro CRDS fox analyser, daily hours of operation.

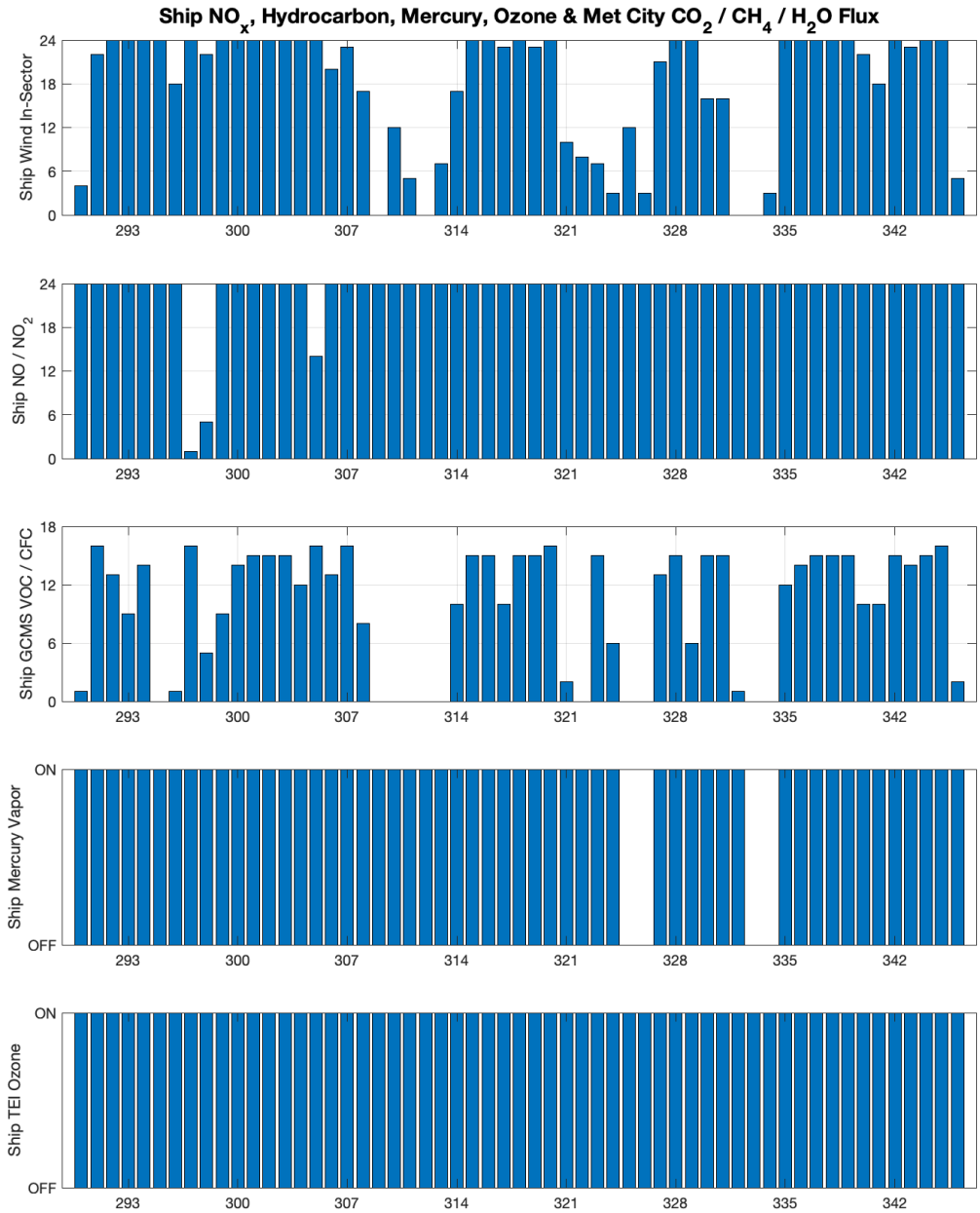

Fig.3.6.4: Other ship analyzers. Top panel: hours per day when the relative wind direction and speed are 'in sector'. Second panel: NO / NO2 analyzer daily hours of operation. Third panel: GCMS, number of samples per day. Fourth panel: Tekran mercury analyzer status (running/not running). Fifth panel: TEI ozone analyzer status (running/not running).

The ship CRDS analyzer and GCMS were operating most of the time when wind conditions were suitable. The mercury, NO/NO_2 and fast and slow ozone systems ran more or less continuously. The DMS APIMS was operating during good wind conditions up to day 322 (18 November), when a DC power supply failed and this could not be repaired. We expect the APIMS will be repaired and running again for Leg 4.

The LI-COR 7500DS on the ship bow tower did not operate reliably during Leg 1. The upper optical element in the analyzer is not heated and was frost covered for almost the entire leg.

Data from this system are mostly useless. When frost conditions ease on later legs we expect usable water vapor flux measurements from this instrument.

Operation of the Met City flux system is not subject to wind sector control. The Met City site was not fully established until day 302. Starting from day 303 the Picarro CRDS ran continuously except for a 12 day period (days 321-332) when ice movement and power failure kept most of the instrumentation at Met City off-line.

The CO_2/CH_4 dynamic chamber flux system was deployed 18 times during Leg 1 and trials of the ozone flux chamber were conducted 6 times, as detailed on Table 3.6.3. Figure 3.6.5 is a time series plot illustrating CO_2 results for a chamber measurement; gas sampling alternates between ambient (inlet) air and air which has circulated through the conical chamber in contact with the surface. After detrending for minor variability in CO_2 concentration in the ambient air, the mean increase or decrease in gas concentration is determined from the repeated measurements. Figure 3.6.2 shows the analyzer box and flux chamber in action.

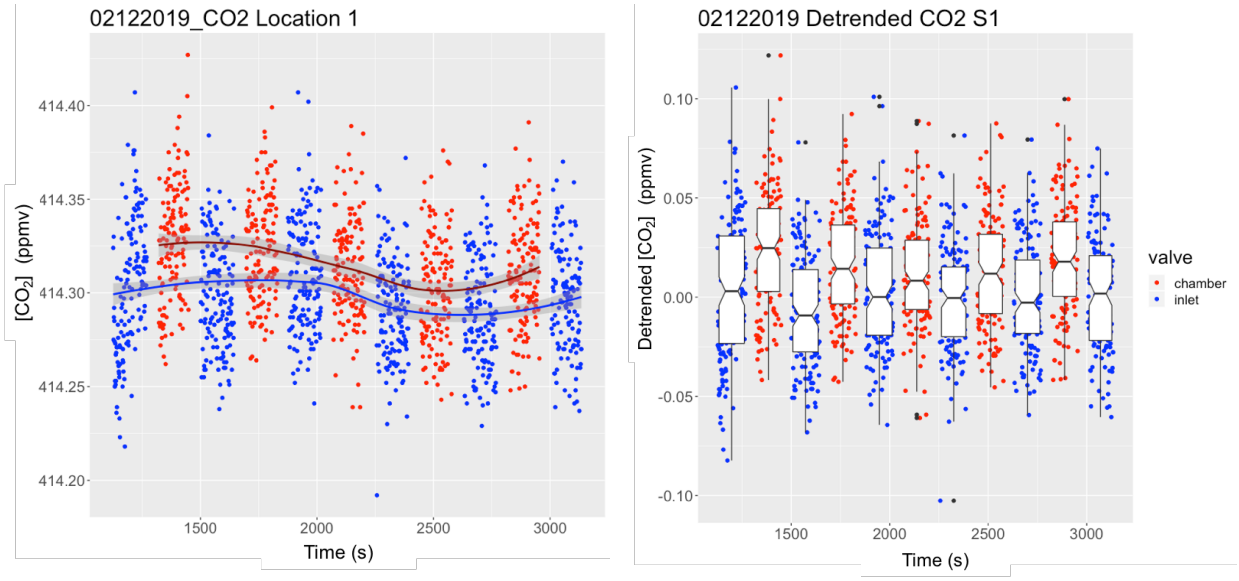

Fig.3.6.5: Example of results from a CO_2/CH_4 dynamic flux chamber deployment. The right panel shows the CO_2 mixing ratio measured in the air entering the chamber (inlet: blue) and air exiting the chamber (chamber: red). Loess fits have been applied to the different sets of data to illustrate the concentration trends. The right panel shows data detrended in relation to the ambient or inlet air. In this case, a significant difference between sequences of inlet and chamber measurements is apparent (T-test, $P = <2.2e^{-16}$) and equates to an emission of CO_2 from the snow/ice to atmosphere of ~ 25 $\mu mol\ m^{-2}\ d^{-1}$.

Tab.3.6.3: Chamber Flux Deployments during Leg 1

Date	DOY	Deployment	Location name
9-Oct-19	282	CO_2/CH_4 Chamber	L3_T1
10-Oct-19	283	CO_2/CH_4 Chamber	L3 T2
27-Oct-19	300	CO_2/CH_4 Chamber	on deck - PS
28-Oct-19	301	CO_2/CH_4 Chamber	Logistics area

Date	DOY	Deployment	Location name
30-Oct-19	303	CO_2/CH_4 Chamber	Met City
3-Nov-19	307	CO_2/CH_4 Chamber	Met City
7-Nov-19	311	CO_2/CH_4 Chamber	BGC_1
11-Nov-19	315	CO_2/CH_4 Chamber	Ice Transect - South
13-Nov-19	317	CO_2/CH_4 Chamber	BGC_3
15-Nov-19	319	CO_2/CH_4 Chamber	Ice Transect - South
20-Nov-19	324	CO_2/CH_4 Chamber	BGC_2
23-Nov-19	327	CO_2/CH_4 Chamber	Dark Site
26-Nov-19	330	CO_2/CH_4 Chamber	Dark Site
27-Nov-19	331	O_3 Flux Chamber	Logistics area
28-Nov-19	332	O_3 Flux Chamber	Logistics area
30-Nov-19	334	CO_2/CH_4 Chamber	Ice Transect - South
1-Dec-19	335	O_3 Chamber	on deck - PS
2-Dec-19	336	O_3 Chamber	Logistics area
2-Dec-19	336	CO_2/CH_4 Chamber	Ice Transect - South
5-Dec-19	339	O_3 Chamber	Logistics area
6-Dec-19	340	CO_2/CH_4 Chamber	BGC 3
7-Dec-19	341	O_3 Chamber	Logistics area
10-Dec-19	344	CO_2/CH_4 Chamber	Ice Transect - South
12-Dec-19	346	CO_2/CH_4 Chamber	Between RS and OC
16-Dec-19	350	CO_2/CH_4 Chamber	Between RS and OC

Data management

All data are handled, documented, archived and published following the MOSAiC data policy (see APPENDIX). Data will be stored at the Arctic Data Centre following the agreement between ADC and the MOSAiC Project lead. DOIs will be communicated to PANGAEA for later access via the future MOSAiC Data Portal.

References

Blomquist BW, Huebert BJ, Fairall CW, Bariteau L, Edson JB, Hare JE, McGillis WR (2014) Advances in air-sea CO2 flux measurement by eddy correlation, Boundary-Layer Meteorol, doi:10.1007/s10546-014-9926-2

Blomquist BW, Huebert BJ, Fairall CW and Faloona IC (2010) Determining the air-sea flux of dimethylsulfide by eddy correlation using mass spectroscopy, Atmos Meas Tech, 3, 1–20, doi:10.5194/amt-3-1-2010

Bariteau L, Helmig D, Fairall CW, Hare JE, Hueber J and Lang EK (2010) Determination of oceanic ozone deposition by ship-borne eddy covariance flux measurements, Atmos Meas Tech, 3, 441–455, doi:10.5194/amt-3-441-2010

3.7 Combined project: (1) formation of secondary nanosized aerosol particles from atmospheric trace gases and ions in the polar marine environment + (2) measurement-based understanding of polar aerosols and their climate effects (MBRACE)

Lauriane Quéléver[1],

(not on board:) Julia Schmale[2], Mikko Sipilä[1], Evo Beck[2], T. Laurila[1], Tuija Jokinen[1], Zoe Brasseur[1], Markus Frey[3], Manuela van Pinxteren[4]

[1]FI.UNI-Helsinki

[2]CH.EPFL

[3]UK.BAS

[4]DE.TROPOS

Objectives

Changes in the arctic sea ice - involving enhancements of its loss rate, mobility, lead opening, or melting pounds – perturb the formation of aerosol, thus clouds, and further impact the climate. The present knowledge about the arctic environment is very limited due to drastic modifications of the polar landscape. Origins as well as chemical and physical mechanisms involved in the formation of aerosol and its later behavior are yet to be resolved. In order to improve the understanding of the changing arctic climate, continuous measurements of aerosol and precursor vapors are performed for a whole annual cycle in the sea ice, herein we present an overview of our measurement deployment for the first phase of the campaign: MOSAiC Leg 1.

Being a collaboration between the Paul Scherrer Institute (PSI) and the Institute for Atmospheric and Earth System research (INAR), this joint project focuses on understanding linkages between (1) sea ice dynamics and thermodynamics, (2) surface and ice characteristics, (3) marine aerosol precursor concentrations and emissions, (4) atmospheric boundary layer dynamics and cloud formation, and finally (5) how all these components vary from polar night (without any radiation from the sun) to arctic summer with all day long solar radiation, thus with an intense and active photochemical potential.

We focus on improving the process level understanding of local aerosol particle formation (sources of trace gases, oxidizing agents) in the polar atmosphere linked to the ecosystem, as well as developing a comprehensive microphysical and chemical characterization of high Arctic aerosol. This results in assessing aerosol transformation mechanisms in the atmosphere and the ability to form both cloud condensation nuclei and ice nuclei.

At the same time, the work identifies periods where the atmosphere exhibits a preindustrial-like aerosol regime as opposed to conditions in which pollution from lower latitudes prevail. Finding the pristine aerosol benchmark in the Arctic will further inform anthropogenic radiative forcing contributions through aerosol-cloud interactions, which rely on the preindustrial state of the atmosphere as reference.

Main questions are:

1. What are the distinctions between pre-industrial pristine Arctic air masses versus those impacted by pollution?
2. What are the roles of different precursors on initial aerosol formation?
3. What is the molecular composition of fresh aerosol particles and how is it affected by precursor emissions?
4. What are the contributions of new particle formation versus long-range transported aerosol to CCN concentrations and what vapors are responsible for the growth to CCN, thus climate relevant sizes?
5. What are the key processes governing the annual cycle of aerosols during different seasons as concerns local sources, long-range transport and scavenging.
6. In which form are Iodine and Sulphur-containing compounds, well known aerosol precursors, emitted from the Arctic Ocean and sea ice, and how do the emissions vary with season or ice characteristics?
7. How is precursor production affected by cosmic rays and photochemistry?
8. How does sea ice as a source of aerosol precursors, secondary aerosol and CCN compare to open polar waters?
9. Does marine and ice biological activity provide different sources of precursors?
10. How do cloud radiative properties depend on the CCN concentration?

Work at sea

Our atmospheric measurements on aerosol and precursor gases was deployed within a laboratory container from the Paul Scherrer Institute operated at the bow of *Polarstern*, at the second container level, forward, starboard side in position C10 (Figure 3.7.1). Several additional filter sampling measurements were made, in the adjacent laboratory container from the British Antarctic Survey (position C9), also supporting filter measurement from TROPOS.

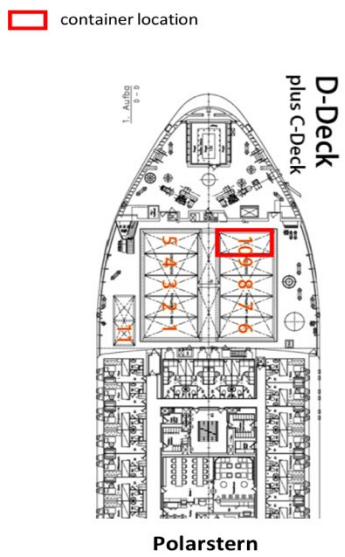

Fig.3.7.1: Location of the C10 container on the Polarstern

Online measurements at the C10 container were performed through three inlets (new particle formation - NPF, interstitial, and total) mounted on the top of the container bringing ambient air into the online instrumentation inside the mobile laboratory. Sampling was continuous with monitoring for local pollution events, via the vessel weather station information (i.e., wind direction and wind speed) from which the data will be segregated during post processing. The collection of instruments includes: various particle counters, size selective particle and ion counters and spectrometers, mass spectrometers, trace gas monitors, filter samplers. An extensive list of the C10 and C9 containers can be found in Table 3.7.1 below.

Tab.3.7.1: Instrumentation deployed during MOSAiC- Leg 1

Id	Instrument	Location - Inlet	Application
CPC 3776	Condensation particle counter	C10 – Total	Aerosol concentration of the total particle population
CPC 3025	Condensation particle counter	C10 - Interstitial	Aerosol concentration of the ultrafine particle population (i.e. diameter < 1 µm)
CPC 3010	Condensation particle counter	C10 – Interstitial & Total	Aerosol concentration of the size selected particle. Used for scanning mobility particle sizer measurement and aerosol mass spectrometer calibration
PSM A11-1 & A11-2	Particle size magnifier	C10 - NPF	Size distribution of the smallest aerosol particles from 1.5 to 3 nm Two identical instruments are run in parallel for scanning and stepping mode inter-comparison
CPC A11-1 & A11-2	Condensation particle counter	C10 - NPF	Used for detection of particle size magnifier setups A11-1 & A11-2
NAIS	Neutral cluster and air ion spectrometer	C10 – NPF	Size distribution of both neutral and naturally charged cluster population for electrical mobility equivalent diameter ranging from 2 to 40 nm
SMPS	Scanning mobility particle sizer	C10 – Interstitial & Total	Size distribution of the aerosol population for electrical mobility equivalent diameter ranging from 10 to 1000 nm
APS	Aerodynamic particle spectrometer	C10 - Total	Size distribution of the large aerosol population for aerodynamic equivalent diameter ranging from 0.5 to 20 µm
CCNC	Cloud condensation nuclei counter	C10 – Interstitial & Total	Aerosol concentration for potential growth cloud condensation nuclei at several supersaturation ratio on hourly cycle
Wibs	Wibs	C10 - Total	Measurement of fluorescently active aerosol for biological speciation

Aethalometer	Aethalometer	C10 – Interstitial & Total	Measurement of black carbon
AMS	Aerosol mass spectrometer	C10 – Interstitial & Total	Chemical compotion of aerosol particle (e.g. sulfate, nitrate, organic, ammonium, chloride, …)
CI-APi-TOF	Nitrate-based chemical ionization atmospheric pressure interface time of flight mass spectrometer	C10 - NPF	Measurement of the chemical composition of gas-phase compound and highly oxidized molecules, precursors of aerosols (e.g. Sulfuric acid, iodic acid, …)
APi-TOF	atmospheric pressure interface time of flight mass spectrometer	C9 - roof	Measurement of the chemical composition of gas-phase naturally charged ions, precursors of aerosols (e.g. Sulfuric acid, ammonia clusters, …)
O3	Ozone monitor	C10 - Interstitial	Ozone concentration
SO2	SO2 monitor	C10 - Interstitial	Sulfur dioxide concentration
Picarro	Picarro Analyzer	C10 - Interstitial	Gas-phase concentration of Methane, Carbon monoxide, Carbon dioxide, water vapor
RH / T 1 & 2	Hygrometer	C10 – Interstitial & Total	Relative Humidity and temperature sensor for both Interstitial and Total inlet
V1	Valve switch	C10 – Interstitial & Total	Hourly bases inlet sample switch for AMS, CCNC, Aethalometer, SMPS
HiVol*	High volume filter sampler	C9 - roof	High volume aerosol filter (Borosilicate, pore ⌀ 1.6 µm 800 Lpm) sampling weekly
LoVol*	Low volume filter sampler	C9 – roof	High volume aerosol filter (Polycarbonate, pore ⌀ 0.2 µm // 20-25 Lpm) automated 48 h cycle sampling
Grimm OPC*	Optical particle counter	C9 – roof	Aerosol concentration of big particles
Filter Tropos**	Filter sampling	C9 – roof	Aerosol filter (Polycarbonate, pore ⌀ 0.8 µm) sampling weekly
*** Support measurement for the British Antarctic Survey (see section 3.8)** **** Support measurement for Tropos**			

One person from the collaborative team participated in the first leg of MOSAiC. Work at sea primarily entailed maintenance and surveillance of online instrumentation to support continuous and proper operation. Daily checks background measurement and calibrations of each instrument were conducted throughout the first leg of the MOSAiC campaign.

Preliminary (expected) results

Results focus on distinguishing local versus long-range aerosol processes for impacting the measured aerosol population. These include unique measurements through different inlets that serve to distinguish aerosol populations, its precursor, properties, and behavior in terms of cloud activity. The suite includes first time measurements of aerosol precursors and nano-sized aerosol particle number concentrations and size distributions from the Arctic Ocean, including concentrations of sulfuric acid, iodic acid, methane sulfonic acid and possible other (highly) oxidized organic compounds (both as naturally charged ions and neutral molecular clusters).

Marking the setup phase of the MOSAiC campaign, and besides the expected pollution events from the ship exhaust fumes, the leg 1 was particularly challenging in term of finding and measuring pristine air masses due to the intense logistic activity preparing the central observatory around the ship. Time series of the total aerosol concentration sampled from both the interstitial inlet (ultrafine particles < 1µm) and the total inlet, from 27 September to 1 December are shown in Figure 3.7.2. In essence, measurements from both particle counters agree (observations validated by the correlation plot in the right panel), which indicate a good reliability of our data but also show a slightly higher concentration of particles from the total inlet at high particle numbers, likely as a result of pollution events, showing that more of the biggest aerosol particles are present in cases of contamination. During the second half of the Leg1, periods of lower particle concentration were seen to occur more often.

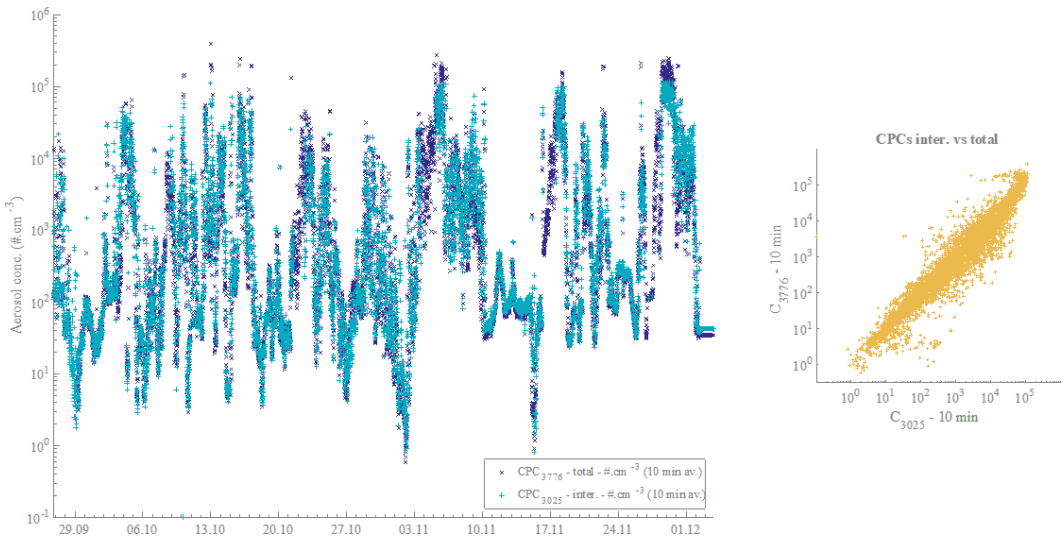

Fig.3.7.2: Left panel: Time series of the total aerosol concentration from 27 September to 1 December measured from the total inlet (dark blue cross) and for the below 1 µm ultrafine particle population from the interstitial inlet (light blue cross). Right panel: Correlation plot between the measurement aerosol concentration between the total inlet and the interstitial inlet. For both plots, the data were averaged on a 10-min time stamp.

During the processing of the data, we will combine the meteorological parameters from the ship weather station (i.e., wind speed, wind direction) cross cut with the logistic operation log (e.g., helicopter flight route) in order to sort the data from pristine measurement conditions from the anthropogenic influence of the MOSAiC deployment that inevitably impact atmospheric measurements. From this starting point the aerosol concentration, properties, composition and also precursor vapors will be thoroughly examined to identify markers of various atmospheric processes.

Data management

All data are handled, documented, archived and published following the MOSAiC data policy (see APPENDIX). Data were collected on measurement instrument computers and backed up to several external hard disks and uploaded weekly on the MOSAiC central server (MCS). The data are delivered and uploaded to the respective institute servers on land after the MOSAiC leg 1. Some data were automatically processed on board (near real time visualization) and some were saved for post campaign processing and analysis. The final data products will be saved and shared publicly after the campaign via PANGAEA (World Data Center PANGAEA Data Publisher for Earth & Environmental Science (www.pangaea.de)).

References

No references

3.8 Sea salt aerosol above arctic sea ice – sources, processes and climate impacts (SSAASI-clim)

Amelie Kirchgässner[1], Lauriane Quéléver[2], Matthew Shupe[3,4]

(not on board:) Markus Frey[1], Thomas Lachlan-Cope[1], X. Yang[1], Alice Jones[1], Leon Clarke[5]

[1]UK.BAS

[2]FI.UNI-Helsinki

[3]EDU.CU

[4]GOV.NOAA

[5]UK.AC.MMU

Objectives

Sea salt aerosol (SSA) influences regional climate directly through scattering of radiation or indirectly via its role as a cloud-forming particle. While it is well known that SSA can be cloud condensation nuclei (CCN) forming cloud droplets, it has been shown only recently that SSA can be also a source of ice nucleating particles (INP) forming ice crystals (DeMott et al., 2016), depending on its chemical composition and surface shape. Aerosol processes and interactions with clouds are very complex (Browse et al., 2014) and Arctic clouds are poorly represented in climate models, which is partly due to a lack of understanding of source and nucleating capability of natural aerosol in the high Arctic. Aerosol models for example do currently not capture aerosol maxima in the Arctic winter/spring observed at high latitudes (e.g. Huang et al., 2017). A recent Antarctic sea ice cruise provided first direct evidence of a source of SSA from salty blowing snow (BSn) above sea ice (Frey et al., 2019), which had been hypothesized previously (Yang et al., 2008): during storms, salty snow gets lofted into the air and then undergoes sublimation to generate SSA. Additional but minor SSA sea ice sources are frost flowers and open leads. Taking into account the blowing snow source of SSA improves model predictions significantly (Yang et al., 2019; Huang et al., 2017). However, the impact on radiation and clouds of SSA from this new sea ice source is not known. And a quantitative understanding of natural aerosol processes and climate interactions is needed to provide a baseline against which to assess anthropogenic pollution reaching the Arctic and evaluate the success of mitigation measures (e.g. AMAP 2015).

This project the SSA source strength is to be determined as well as fate and potential impact on Arctic climate associated with blowing snow above sea ice and other sea ice sources. A particular focus is on quantifying the contribution of ice nucleating particles (INP) from sources related to Arctic snow and sea ice. Participation in the year-long MOSAiC expedition provides the unique opportunity to observe key aerosol processes and properties in the central Arctic Ocean throughout all seasons of the year.

The first objective is to quantify SSA variability above sea ice and relative contributions from local sources (blowing snow, frost flowers and open leads) throughout the year. This will be achieved through (a) in-situ measurements of particle size distribution and concentration, covering all relevant sizes ranging from the sub-micron scale to the scale of airborne snow particles at various levels within the atmospheric boundary layer and in the free troposphere using a tethered balloon platform. And (b) through chemically fingerprinting the local snow and sea ice source using major ion ratios and sulfur isotopes, and compare these to the chemical composition of aerosol to constrain its contribution to Arctic SSA.

The second objective is to quantify the contribution of SSA above sea ice to cloud forming particles. This will be achieved through (a) measurement of ice nucleating particles (INP) in the air above the sea ice to evaluate their variability associated with SSA concentrations and events (blowing snow, opening of leads). And (b) through testing for the presence of INP in snow on sea ice, brine, frost flowers and link to ambient INP.

The third objective is to determine the climate sensitivity to SSA from the sea ice source (blowing snow, frost flowers, open leads) in the Arctic through numerical modeling based on existing and new MOSAiC observations. This will be achieved through (a) quantification of the direct radiative effect of SSA and (b) quantification of the indirect radiative effect of SSA via its contributions to INP/CCN and their impact on cloud fraction.

Work at sea

Activities were conducted at multiple locations across the MOSAiC observatory and generally supported by other groups (see sections 3.4 and 3.7). At Met City, the CLASP instrument was installed at about 3m height on the 11m mast and data is being logged with the University of Colorado flux team data (see section 3.4). Additionally, two snow particle counters (SPCs) were installed on the 11-m tower, sampling at a height near the surface and at about 10m to observe blowing snow particle concentrations. Near Met City, rocket traps were set up to capture blowing snow for physical sample analysis of blowing snow. Onboard, the BAS lab container was installed at position C9 on the bow of *Polarstern*. This container served as the base of operations for filter and particle counter samples that were supported by the INAR team (see section 3.7). These included a high volume filter (borosilicate, pore size of 1.6 mm, 800 L/min, with weekly sampling), and a low volume filter (polycarbonate, pore size of 0.2 mm, 20-25 L/min, automated 48h sampling), which will be used to support laboratory analyses of ice nucleating particle concentrations and particle chemical composition. In addition, an online Grimm optical particle counter for tracking the concentration of large aerosols.

Preliminary (expected) results

No direct results have been obtained yet, although data sets and samples are ready for future analyses. The datasets of SSA and INP above sea ice, as well as chemical source signature of snow and sea ice from the Central Arctic Ocean will provide important insights into Arctic sea ice as a particle source. They will lead to improved model parameterisations of the SSA blowing snow source as a function of sea ice properties, as well as a better understanding of the potential impact on Arctic clouds. And finally, SSA is also a potential sea ice proxy measured in polar ice cores (Abram, et al., 2013) and quantifying the SSA sea ice source will constrain reconstructions of past Arctic sea ice conditions (e.g. Rhodes et al., 2017).

Data management

Online measurements will be available soon after completion of the MOSAiC cruise in 2020, whereas data from the off-line chemical analysis of aerosol filter, snow and ice samples will become available after completion of lab analysis in the UK by mid 2021. All SSAASI-CLIM data will be made available within the MOSAiC data management framework and will

eventually be archived at the British Polar Data Centre and DOIs communicated to PANGAEA for later access via the future MOSAiC Data Portal, according to the protocol agreed upon between these two archives. All data are further handled, documented, archived and published following the MOSAiC data policy. Exceptions are documented in written agreements between the data provider and the MOSAiC Project Board and data manager.

References

Abram NJ, Wolff EW, Curran MA (2013) A review of sea ice proxy information from polar ice cores, Quaternary Science Reviews, 79, 168 – 183, doi:10.1016/j.quascirev.2013.01.011.

AMAP Assessment 2015, Arctic Monitoring and Assessment Programme, vii + 116 pp..

Browse J, Carslaw KS, Mann GW, Birch CE, Arnold SR, Leck C (2014) The complex response of Arctic aerosol to sea-ice retreat, Atmospheric Chemistry Physics, 14, 7543–7557, doi:10.5194/acp-14-7543-2014.

DeMott PJ, and Coauthors (2016) Sea spray aerosol as a unique source of ice nucleating particles, Proc. of the National Academy of Sciences, 113, 5797–5803, doi:10.1073/pnas.1514034112.

Frey MM, Norris SJ, Brooks IM, Anderson PS, Nishimura K, Yang X, Jones AE, Nerentorp Mastromonaco MG, Jones DH, Wolff EW (2019) First direct observation of sea salt aerosol production from blowing snow above sea ice, Atmospheric Chemistry Physics. Disc., doi:10.5194/acp-2019-259.

Huang J, Jaeglé L (2017) Wintertime enhancements of sea salt aerosol in polar regions consistent with a sea ice source from blowing snow, Atmospheric Chemistry Physics, 17, 3699–3712, doi:10.5194/acp-17-3699-2017.

Rhodes RH, Yang X, Wolff EW, McConnell JR, Frey MM (2017) Sea ice as a source of sea salt aerosol to Greenland ice cores: a model-based study, Atmospheric Chemistry Physics, 17, 9417–9433, doi:10.5194/acp-17-9417-2017.

Yang X, Frey MM, Rhodes RH, Norris SJ, Brooks IM, Anderson PS, Nishimura K, Jones AE, Wolff EW (2019) Sea salt aerosol production via sublimating wind-blown saline snow particles over sea ice: parameterizations and relevant microphysical mechanisms, Atmospheric Chemistry Physics, 19, 8407–8424, doi:10.5194/acp-19-8407-2019.

Yang X, Pyle JA, Cox RA (2008) Sea salt aerosol production and bromine release: Role of snow on sea ice, Geophysical Research Letters, 35, doi:1029/2008GL034536.

3.9 Evaluation of ice nucleating particles and their sources in the central arctic during MOSAiC

Jessie Creamean[1] [1]EDU.CSU

(not on board:) Paul DeMott[1], Thomas Hill[1]

Objectives

The accelerated rate of warming in the Arctic is of great concern due to potential impacts that include release of greenhouse gases from permafrost, melting glacial ice contributing to sea level rise, and declining sea ice cover exposing the darker ocean surface. These processes induce positive feedbacks and contribute to further warming that affects climate globally. Clouds play a crucial role in regulating the energy reaching the sea ice and snow surfaces, but the magnitude of their effects on surface temperature is not well constrained in the Arctic. Aerosols are also an important contributor by serving as seeds for cloud particle formation, but even less is known about their overall impact and origin, especially aerosols that factilitate cloud ice formation (called ice nucleating particles or INPs).

The overarching goal of this project is to achieve unprecedented characterization of INP abundance and sources (including biological) to evaluate their capacity to modulate cloud ice

formation over the central Arctic. Specifically, the work is organized under three main objectives:

Objective 1: Process size-resolved and total aerosol samples collected during MOSAiC for quantitative INP measurements and aerosol microbiological characterization to produce a high-quality dataset to be made available to the scientific community.

Objective 2: Coordinate collection of seawater, surface microlayer (SML), snow, and sea ice samples for assessment of local INP sources to leverage complimentary aerosol INP measurements (see section 6 of this cruise report for details).

Objective 3: Address a set of targeted scientific research questions based on current gaps in the understanding of INPs in the central Arctic:

- How do seasonal changes in sea ice and air mass transport influence INP abundance and sources in the central Arctic?
- Are marine and sea ice biological processes a significant source of atmospheric INPs as compared to terrestrial sources?
- Are open water environments such as leads and melt ponds viable sources of INPs over the sea ice and do such environments exchange INPs with the atmosphere?

This project is funded by the US Department of Energy Atmospheric System Research and Atmospheric Radiation Measurement Programs.

Work at sea

The aerosol sampling activities during Leg 1 involved deployment of: 1) a size-resolved DRUM (DRUMAir™) and 2) two disposable sterile filter units (Nalgene™) per 72-hour sampling period, both for continuous collection of time-resolved aerosol samples during MOSAiC. These samplers were integrated into and outside of the second ARM Mobile Facility (AMF2) container. The DRUM collects aerosol particles at four size ranges (i.e., from 0.15 to > 12 µm in diameter with size cuts at 2.96, 1.21, and 0.34 µm). This size range covers a wide array of aerosols—particularly those that serve as INPs. Aerosols were impacted on clean perfluoroalkoxy substrate strips coated with petrolatum, a material tested by PI Creamean containing very few artifacts that interfere with INP analysis. The substrate strips were adhered to discs in each size chamber that rotate slowly over time, developing a “smear” of aerosol loading. After 24 hours, the discs rotated an additional 2 mm quickly, leaving a blank spot in between each daily sample. The DRUM continuously collected 24-hour samples for approximately 25 days without changing the substrates. The two filter units for multi-day integration of aerosols were comprised of a vacuum pump pulling air through polycarbonate filters (0.2 and 0.4 µm) fitted within sterile filter units covered by precipitation shields.

Aerosol filter and substrate samples collected during Leg 1 were stored frozen at –20 °C on *Polarstern* and transferred frozen to Colorado State University (CSU) where they will be stored frozen until analysis.

Additional sampling activities included collection of seawater, sea ice, and snow to assess the local sources of INPs (i.e., called “source” samples) and are described in detail in section 6.

Preliminary (expected) results

Preliminary INP data are not available because all sample processing will be conducted offline at CSU. Table 3.9.1 describes the sampling statistics for aerosol INPs for leg 1.

Tab.3.9.1:

Sample type	Frequency	Total # of samples

DRUM aerosol	24-hour	53
Filter unit aerosol	72-hour	34
TOTAL:		87

In the upcoming months, samples will be subject to processing for INPs using two established immersion freezing ice nucleation techniques—the DRUM and filter samples will be processed with the CSU drop freezing cold plate (CP) and CSU ice spectrometer (IS), respectively. A subset of the DRUM samples will be processed for time- and size-resolved INPs using the CP to manifest a semi-continuous time series of INPs during the annual cycle. One of the filter units will be processed for offline immersion INPs using the IS and one for DNA sequencing (i.e., amplification of select regions of the 16S and 18S genes) to assess the total INP time series and presence of possible biological ice nucleators. A further subset of samples from the first filter unit will be subject to heat and peroxide treatments to afford information on proteinaceous and organic INPs, respectively.

Immersion freezing—whereby an INP is immersed in a water droplet via activation of CCN followed by droplet freezing at subzero temperatures—is the most relevant to AMPC formation. Drop freezing assays are a widely-used technique for immersion mode ice nucleation measurements. Once ready for processing, DRUM substrate strips will be carefully cut into segments to yield daily samples, as done during previous field deployments. A subset of these samples will be analyzed, while the remainder will be stored frozen in sterile Whirl-Pak® bags. The substrate segments for immediate processing will be added to 2 mL of ultrapure water in sterilized 50-mL beakers, then mixed using a vortex mixer for at least 1 hour at 500 rpm to resuspend particles from the petrolatum into the solution. Following sample preparation, 100 2.5-µL aliquots will be created on a 3-inch diameter copper plate and covered to prevent contamination. The plate is cooled at approximately 1 – 10 °C min^{-1} from room temperature until all drops freeze on the plate or until the CP limit of approximately –35 °C. Drop freezing is detected and recorded through monitoring software to provide the freezing temperature and cooling rate for each drop. Each sample will be tested three times (i.e., a new set of 100 drops created for each test).

The IS is an immersion freezing measurement device with well-established, documented experimental protocols. For processing, the 0.2-µm filter from each sampling set is placed in 50-mL sterile polypropylene tubes with 8 mL of 0.1-µm filtered deionized water and shaken at 200 rpm for 20 min to resuspend particles. The IS consists two 96-well aluminum blocks designed for incubations of PCR (polymerase chain reaction) plates placed end-to-end and encased, on their sides and base, by cold plates. Aliquots of the aerosol suspension are dispensed into PCR trays (under a laminar flow clean hood), the trays are placed in the blocks, the device is covered with a plexiglass window, and the headspace purged with N_2. Frozen aliquots of 50 µL are counted at 0.5 °C intervals as temperature is lowered at ~0.33 °C min^{-1} to –27 °C. Serial dilutions in deionized water are used to count INPs active at the lowest temperatures. Three IS instruments, semi-automated for aliquot freezing through interface with a CCD camera system and control with LabVIEW (NI, Inc.), are available for use. We propose to further characterize portions of suspensions of aerosol samples using treatments to isolate biological and organic versus inorganic INPs. This is the special advantage of performing IS processing in addition to DRUM-CP processing. The stability (or lack thereof) of INPs to these treatments provides an indication of composition. To assess the fractional contribution of heat labile (i.e., biological) entities, such as proteinaceous INPs, a 1.5-mL aliquot of suspension is re-tested after heating to 95 °C for 20 min. To remove all organic INPs (marine and terrestrial), 0.75 mL of 30% H_2O_2 is added to a 1.5-mL aliquot of suspension and the mixture heated to 95 °C for 20 min while illuminated with UVB fluorescent bulbs to generate hydroxyl radicals

(residual H_2O_2 is removed using catalase), and the INPs are again assessed in the IS. Remaining INPs are likely to be mineral.

From the fraction of drops frozen and the known total volume of air/water per sample for both techniques, we can calculate the estimated INP concentration with a universally-used equation by Vali:

$$K(\theta)\ (L^{-1}) = \frac{\ln\,(1-f)}{V_{drop}} \times \frac{V_{suspension}}{V_{air}}$$

where f is the proportion of droplets frozen, V_{drop} is the volume of each drop, $V_{suspension}$ is the volume of the suspension, and V_{air} is the volume of air per sample. Additionally, since we will have size-resolved INPs and surface area (from sizing instruments), we can calculate the number of ice nucleation active sites (n_s), which has been more recently used to describe ice nucleation efficiency of particles. Procedural controls of the sampling substrates will provide quantitative information on the signal to noise ratio to correct for background artifacts.

Data management

All data from this project will be treated and archived according to the DOE ARM protocols outlined in section 3.2.

References

No references